




# Identifiable Solutions to Foreground Signature Extraction From Hyperspectral Images in an Intimate Mixing Scenario

Jarrold Hollis , Raviv Raich , *Senior Member, IEEE*, Jinsub Kim , *Member, IEEE*, Barak Fishbain , and Shai Kendler 

**Abstract**—Hyperspectral imaging considers the measurement of spectral signatures in near and far field settings. In the far field setting, the interactions of material spectral signatures are typically modeled using linear mixing. In the near field setting, material signatures frequently interact in a nonlinear manner (e.g., intimate mixing). An important task in hyperspectral imaging is to estimate the distribution and spectral signatures of materials present in hyperspectral data, i.e., unmixing. Motivated by forensics, this work considers a specific unmixing task, namely, the problem of foreground material signature extraction in an intimate mixing setting where thin layers of foreground material are deposited on other (background) materials. The unmixing task presents a fundamental challenge of unique (identifiable) recovery of material signatures in this and other settings. We propose a novel model for this intimate mixing setting and explore a framework for the task of foreground material signature extraction with identifiability guarantees under this model. We identify solution criteria and data conditions under which a foreground material signature can be extracted up to scaling and elementwise-inverse variations with theoretical guarantees in a noiseless setting. We present algorithms based on two solution criteria (volume minimization and endpoint member identification) to recover foreground material signatures under these conditions. Numerical experiments on real and synthetic data illustrate the efficacy of the proposed algorithms.

**Index Terms**—Endmember extraction, hyperspectral imaging, identifiability, intimate mixing model, nonlinear unmixing.

## I. INTRODUCTION

THE hyperspectral unmixing problem has applications in endmember signature extraction [2], [3] and classification [4], [5] tasks. A pixel from a hyperspectral image may be viewed as a mixture of the spectral signatures from materials located within the spatial bounds of the pixel. In remote sensing, mixtures are commonly described as non-negative linear combinations of spectral signatures weighted by the proportions of the pixel covered by each corresponding material. This setting gives rise to the linear mixing model, for which several approaches to solving the unmixing problem have been proposed [2], [3], [6]. Other works have explored settings in which nonlinear effects, such as reflection and refraction, have a non-negligible effect on the spectral mixtures represented by each pixel. There are a wide range of potential nonlinear unmixing models [7], [8], and dedicated algorithms for cases where the measured signature is noisy [9], [10], [11].

**Linear mixing model** The task of extracting material signatures has been one of the key challenges in the linear mixing model. The measurement model for this setting is

$$\mathbf{y}_p = \sum_{r=1}^R \alpha_{r,p} \mathbf{m}_r, \quad (1)$$

where measurement  $\mathbf{y}_p \in \mathbb{R}^M$  of pixel  $p$  (taken over  $M$  wavelengths) is expressed as a non-negative linear combination of the  $R$  distinct material signatures, or *endmembers*,  $\mathbf{m}_1, \mathbf{m}_2, \dots, \mathbf{m}_R \in \mathbb{R}^M$ , weighted by their *abundances*  $\alpha_{1,p}, \alpha_{2,p}, \dots, \alpha_{R,p}$  (see [12], [13], [14]). Proposed unmixing methods based on a geometric approach are of particular relevance to our work. Geometric approaches can be categorized into pure pixel based methods and volume minimization methods. Pure pixel based methods utilize the *pure pixel* assumption, where the data to be unmixed is assumed to contain at least one pixel for each endmember containing only that endmember. Methods such as the pixel purity test [15], N-FINDR [2], VCA [13], and AVMAX [16] reduce to finding such pure pixels. Volume minimization based methods find a minimum volume simplex that encloses all pixels in the data; the endmembers are the vertices of the obtained simplex. Methods such as MVES [17] and MinVolNMF [18] enforce the enclosure of pixels as a hard constraint, while other methods such as MVSA [19] and SISAL

Manuscript received 14 November 2023; revised 1 February 2024, 2 April 2024, and 9 May 2024; accepted 15 May 2024. Date of publication 29 May 2024; date of current version 24 September 2024. This work was supported in part by Israel Ministry of Science and Technology Research Program and in part by Israel Ministry of Environmental Protection. An earlier version of this paper was presented at the IEEE International Conference on Acoustics, Speech and Signal Processing (ICASSP), 2020 [DOI: 10.1109/ICASSP40776.2020.9053456]. The associate editor coordinating the review of this manuscript and approving it for publication was Prof. Charles Soussen. (*Corresponding author: Jarrod Hollis.*)

Jarrold Hollis, Raviv Raich, and Jinsub Kim are with the School of Electrical Engineering and Computer Science, Oregon State University, Corvallis, OR 97331 USA (e-mail: hollisj@oregonstate.edu).

Barak Fishbain is with the Environmental, Water and Agricultural Engineering Division, Technion-Israel Institute of Technology, Haifa 32000, Israel.

Shai Kendler is with the Faculty of Civil & Environmental Engineering, Water and Agricultural Engineering, Rabin Hall, Technion Israeli Institute of Technology, Haifa 32000, Israel.

This article has supplementary downloadable material available at <https://doi.org/10.1109/TSP.2024.3406714>, provided by the authors.

Digital Object Identifier 10.1109/TSP.2024.3406714

[6] attempt to account for noise by allowing negative abundance estimates with some penalty term. Geometric approaches based on volume minimization do not require the pure pixel assumption to be satisfied, but other data conditions may be necessary. Non-geometric approaches are also developed in the literature, such as sparsity constrained approaches or statistical approaches. Methods such as  $L_{1/2}$ -NMF [20] and MLNMF [21] are variants of NMF algorithms with different choices of constraints to enforce sparsity in abundance coefficients (and on endmembers of each layer in the case of MLNMF). SUnSAL and C-SUnSAL [22] are based on the alternating direction method of multipliers, and enforce yield sparse abundance coefficient estimates. In [23], a distributed approach is suggested which enforces both sparsity constraints and encourages consistency in endmember abundances in neighborhoods of pixels. In [24], the distributed approach is extended by forming neighborhoods via fuzzy  $c$ -means clustering as a processing step. Tensor factorization methods have also been suggested for preserving and/or utilizing spatial information in unmixing [25], [26]. For additional references on linear unmixing, we refer the reader to [12] and [27], and the references therein.

**Bilinear mixing model** Generalizations of the linear mixing model to address nonlinear mixtures of signatures are also considered, such as the bilinear mixing model introduced in [28]. The measurement model is

$$\mathbf{y}_p = \sum_{r=1}^R \alpha_{r,p} \mathbf{m}_r + \sum_{i=1}^R \sum_{j=i}^R \beta_{i,j,p} \mathbf{m}_i \odot \mathbf{m}_j, \quad (2)$$

where the measurement  $\mathbf{y}_p \in \mathbb{R}^M$  is expressed as a linear combination of the material signatures  $\mathbf{m}_1, \mathbf{m}_2, \dots, \mathbf{m}_R \in \mathbb{R}^M$  weighted by the linear abundances  $\alpha_{1,p}, \alpha_{2,p}, \dots, \alpha_{R,p}$ , and a linear combination of pairwise products of these material signatures weighted by the bilinear abundances  $\beta_{1,1,p}, \beta_{1,2,p}, \dots, \beta_{R,R,p}$ .

Several methods have been proposed for solving the bilinear unmixing problem in a *supervised* setting. In [28], material signatures are obtained via an oracle (using either label information or expert identification). A material signature matrix is formed with columns containing both the previously identified endmembers and their bilinear combinations, and abundances are then estimated by solving a constrained linear least squares problem as in the linear mixing model (see [14]). In [29], it is similarly assumed that endmembers are available directly. Estimates of the abundances for the linear and bilinear combinations are obtained with an alternating minimization of a fitting error objective, alternating between updates for abundances of each type of combination. The iterative update with respect to each parameter has the form of a semi-NMF (non-negative matrix factorization) problem and is solved using existing algorithms [30]. In [31], material signatures are again assumed to be given or estimated via existing algorithms for the linear unmixing problem, such as the pixel purity test or N-FINDR. The abundance coefficients are then obtained via Bayesian estimation, where priors are derived from the constraints on the abundance coefficients and from assumed additive Gaussian random noise in the data.

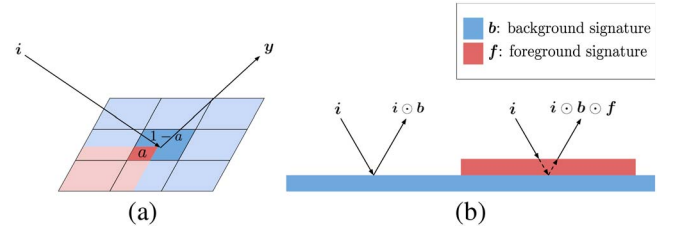


Fig. 1. Visualizations of the intimate mixing model described in (3). Indexing by  $p$  is omitted. (a) Example of fractional coverage by the foreground material. (b) Effect of background only vs background and foreground.

Some works have explored the bilinear unmixing problem in an *unsupervised* setting. In [32], it is proven that spectral endmembers can be identified up to the typical variations of scaling and permutation under certain conditions, namely: all interactions of endmembers are observed in the data, and the number of pixels in the data is  $O(R^4)$ , where  $R$  is the number of endmembers in the data. In [33], the requirement that all interactions of endmembers are observed in the data is instead relaxed to a “near-separable” condition, which is equivalent to the pure pixel assumption for endmembers.

**Other nonlinear mixing models** Other nonlinear mixing models besides the bilinear mixing model have been explored in the literature. Various forms of intimate mixing models have been explored, such as the Hapke model [34] or the intimate mixing model with foreground and background materials in [9] (see Equation (4)). Some works have explored more general nonlinear mixing frameworks, such as [35]. For additional references on bilinear and other nonlinear unmixing approaches, we refer the reader to [7] and the references therein.

**Proposed intimate mixing model** In this paper, we consider the non-linear intimate mixing scenario of [9] in which a thin layer of foreground material is deposited on the surface of other (background) materials. In this setting, the measurement of each pixel is modeled as a nonnegative linear combination of the spectral signature from a background material and the product of the spectral signatures from a foreground material and the background material (see Fig. 1). The model is expressed as

$$\mathbf{y}_p = (\mathbf{i}_p \odot \mathbf{b}_p) \odot (a_p \mathbf{f}_p + (1 - a_p) \mathbf{1}), \quad (3)$$

where  $\mathbf{f} \in \mathbb{R}^M$  is the foreground material signature (with  $M$  entries corresponding to different frequency bands),  $\mathbf{b}_p \in \mathbb{R}^M$  is the background material signature,  $\mathbf{i}_p \in \mathbb{R}^M$  is the reference illumination, and  $a_p$  is the foreground material coverage. The notation  $\mathbf{u} \odot \mathbf{v}$  indicates the Hadamard (element-wise) product between same-sized vectors  $\mathbf{u}$  and  $\mathbf{v}$ . As these quantities represent physical phenomena, the material and illumination signatures are strictly positive, and the coverage coefficient satisfies  $a_p \in [0, 1]$ . In [10], this setting is used to model the detection of suspicious material in envelopes. Our task of interest is to extract the foreground material signature from a set of pixels following the intimate mixing model. This is an unsupervised problem; no a priori information of the material signatures or the material distributions within the set of pixels is assumed.

To facilitate this task, we consider some modeling assumptions. We assume only one foreground material is present. Similar to [9] and [36], we assume that the background material is nearly invariant within small neighborhoods of pixels  $\mathcal{N}_k$  (henceforth referred to as *patches*) for  $k = 1, \dots, K$  such that each patch contains exactly one background material. In [10], reference illumination is assumed to be spatially-invariant; we consider per-pixel scaling of illumination to account for attenuation from physical phenomena such as shadowing. Under these assumptions, the intimate mixing model reduces to our *bag-of-patches* model, and can be expressed for the measurement of pixel  $p$  as

$$\mathbf{y}_p = K_p(\mathbf{i} \odot \mathbf{b}_k) \odot (a_p \mathbf{f} + (1 - a_p)\mathbf{1}), \quad p \in \mathcal{N}_k, \quad (4)$$

where  $K_p$  is the non-negative scaling factor for illumination. In practice, patches may be obtained by sampling small regions of pixels such that the assumption of a nearly invariant background material signature holds. Even with these assumptions, multiple solutions may be found when trying to extract the foreground material signature from data following the bag-of-patches model due to the redundancy associated with the model parameterization and the non-linearity of the model. For example, the illumination and background material signature parameters cannot be uniquely resolved from their product. Further, pixels fit by the model are dependent on the product of foreground and background material signature parameters. The non-linearity of the model means that existing linear unmixing methods cannot be applied directly to this problem, and that uniqueness conditions for the linear mixing model cannot be applied.

The intimate mixing model we consider in this paper can be seen as particular case of the bilinear mixing model, and the foreground material signature extraction problem is related to the bilinear unmixing problem in the unsupervised setting. We note that previously proposed methods for bilinear unmixing in the unsupervised setting are not suitable for our method. The BMMF-LS-NM method proposed in [32] requires that all interactions of endmembers are observed in data, but in the intimate mixing model we consider the interactions between different background signatures are not observed. The SNPALQ method proposed in [33] requires that each endmember appear as a pure pixel in the data, but in the intimate mixing model we consider, foreground materials can never appear as pure pixels and must always be mixed with background materials. The lack of applicable existing methods motivates us to identify criteria and conditions suitable for our model of interest under which foreground material signatures can be extracted.

Identifiability analysis of the unmixing problem is a fundamental challenge. For the *linear mixing model*, material signatures are said to be identifiable if they can be identified up to some trivial ambiguities (i.e., scaling and permutation) based on the data. There are some known sufficient data conditions that ensure the identifiability of the material signatures. One such condition is *separability* [37], [38]: each material signature must appear in isolation in at least one pixel (referred to as *endmembers*). Such pixels are referred to as endpoints. For a

single patch under our proposed model, this would be equivalent to the patch containing a pixel with no foreground material and a pixel entirely covered with foreground material. A more relaxed condition known as sufficient scattering has also been proposed [39], [40].<sup>1</sup> It has been shown that under the aforementioned data conditions for the linear mixing model, algorithms such as MinVolNMF [18] can recover the true material signatures. To our knowledge, no works have developed equivalent identifiability conditions for the bilinear mixing model.

In this paper, we focus on *unsupervised* extraction of the foreground signature in the intimate mixing model with identifiability guarantees. We note that the intimate mixing model (4) may be viewed as a special case of the linear mixing model and the bilinear mixing model. However, the existing signature extraction approaches for the linear and bilinear mixing models are not readily applicable to our problem. For instance, the signature extraction methods for the linear mixing model (1) could be viable approaches if we are given a patch  $\mathcal{N}_k$  that contains two endpoint pixels, i.e., one pixel data being a scalar multiple of  $\mathbf{i} \odot \mathbf{b}_k$  and another pixel data being a scalar multiple of  $\mathbf{i} \odot \mathbf{b}_k \odot \mathbf{f}$ . In such a case, the separability condition for the linear mixing model is satisfied by this patch, and thus any signature extraction approach for the linear model can be applied to this patch to identify the two endmembers,  $\mathbf{e}_1 = \mathbf{i} \odot \mathbf{b}_k$  and  $\mathbf{e}_2 = \mathbf{i} \odot \mathbf{b}_k \odot \mathbf{f}$ , which can be used to obtain  $\mathbf{f}$ . However, in practice there is no guarantee that a patch with two endpoint pixels would exist. Furthermore, even when such a patch exists, its identity is unknown and difficult to infer due to the variation of background material signatures across patches. The intimate mixing model (4) can also be seen as a special instance of the bilinear mixing model (2) after proper reparameterization. However, it does not lead to a viable solution approach due to the lack of unsupervised signature extraction approaches for the bilinear model. We also note that existing methods for unmixing in the bilinear mixing model do not have identifiability guarantees. Such guarantees are necessary for foreground signature extraction, where the true foreground material signature is potentially unknown and, therefore, not verifiable with an external oracle. The main contributions of this paper are:

- 1) Introduction of a bag-of-patches model for the intimate mixing problem, and characterization of the solution space for the problem;
- 2) Development of identifiability data conditions for solutions of the foreground material signature under the bag-of-patches model. We show that, under appropriate data conditions, solutions satisfying the minimum volume and/or endpoint fit properties will match the true foreground material signature up to variations of scaling and element-wise inversion. In contrast to existing identifiability data conditions requiring two endmembers in every patch, the proposed condition requires only two endmembers among *all* patches;

<sup>1</sup>In the intimate mixing model, the sufficient scattering condition is equivalent to the separability condition.



- 3) Proposal of algorithms based on the proposed identifiability criteria to find solutions under this model with identifiability guarantees. One algorithm considers a volume minimization criterion, and the other algorithm is based on an endpoint identification approach.

This paper extends our previous work, “Foreground signature extraction for an intimate mixing model in hyperspectral image classification”, originally presented in ICASSP 2020 [1]. The previous work introduced the bag-of-patches model, proposed a volume minimization-based algorithm for foreground signature extraction, and suggested (without proof) a strong data-based condition (strict-tightness) under which the volume-minimization algorithm would be successful. In contrast, this paper introduces a relaxed data condition which generalizes the strict-tightness condition, provides formal identifiability analysis with proofs for this data condition, introduces an additional algorithm based on endpoint identification, and includes additional experiments on synthetic data as well as evaluations against several benchmark algorithms.

The remainder of this paper is organized as follows. The observation model and the associated foreground material signature extraction problem are described in Section II. Conditions under which an identifiable solution for a foreground material signature can be obtained are developed in Section III. Section IV presents our proposed algorithms based on the previously identified conditions. The performance of our proposed methods is evaluated with numerical experiments on synthetic data. The process and results are given in Section V, and conclusions and future works are stated in Section VI. Proofs of the various theoretical results in the paper are given in the appendix and supplementary material.

## II. PROBLEM SETUP AND CHALLENGES

We introduce a summary of notations used in the paper. We then proceed with a formal description of our problem, including the intimate mixing model, our proposed bag-of-patches model, and the ambiguity of representation in this model.

### A. Notations

In this paper, small letters (both roman and greek) are used to denote scalars (e.g.,  $a$ ,  $\alpha$ ), boldface small letters (both roman and greek) are used to denote column vectors (e.g.,  $\mathbf{v}$ ,  $\boldsymbol{\theta}$ ), and boldface capital letters are used to denote matrices (e.g.,  $\mathbf{M}$ ). The Hadamard product and division between two vectors is denoted  $\mathbf{u} \odot \mathbf{v}$  and  $\mathbf{u} \oslash \mathbf{v}$ , respectively, for same sized vectors  $\mathbf{u}$  and  $\mathbf{v}$ . The element-wise matrix inequality is denoted  $\mathbf{A} \geq c$  for arbitrarily sized matrix  $\mathbf{A}$  and scalar  $c$ .

### B. Bag-of-Patches Model

Recall the intimate mixing bag-of-patches model introduced in (4). This model has many sources of ambiguity: the scaling factors and coverage coefficients are not separable, as well as the reference illumination and each background material signature. The unique identification of these parameters is not

relevant to the task of foreground material signature extraction, so we consider the following reparameterization: let  $c_{1,p} := K_p a_p$ , let  $c_{2,p} := K_p(1 - a_p)$ , and let  $\mathbf{v}_k := \mathbf{i} \odot \mathbf{b}_k$ . Note that the restrictions of  $K_p$  and  $a_p$  (i.e.,  $K_p \geq 0$  and  $a_p \in [0, 1]$ ) require that each  $c_{1,p}$  and  $c_{2,p}$  also be non-negative. Similarly, the strict positivity of  $\mathbf{i}$  and  $\mathbf{b}_k$  require that  $\mathbf{v}_k$  be strictly positive. The reformulated bag-of-patches model can be expressed as

$$\mathbf{Y}^{(k)} = \text{diag}(\mathbf{v}^{(k)}) [\mathbf{f} \ \mathbf{1}] \mathbf{C}^{(k)}, \quad \mathbf{v}^{(1)}, \dots, \mathbf{v}^{(K)}, \mathbf{f} > 0, \quad \mathbf{C}^{(k)} \geq 0, \quad (5)$$

where  $N_k$  is the number of pixels in each patch, each patch  $\mathbf{Y}^{(k)}$  is an  $M \times N_k$  matrix with  $\mathbf{Y}^{(k)} := [\mathbf{y}_1 \ \dots \ \mathbf{y}_{N_k}]$ ,  $\mathbf{f}$  and each  $\mathbf{v}^{(k)}$  are  $M \times 1$  vectors, and each  $\mathbf{C}^{(k)}$  is a  $2 \times N_k$  matrix with  $[\mathbf{C}^{(k)}]_{ij} := c_{i,j}^{(k)}$ . We further require that each patch  $\mathbf{Y}^{(k)}$  is rank 2.<sup>2</sup>

### C. Problem Formulation

Given a collection of hyperspectral data  $\mathbf{Y}^{(1)}, \dots, \mathbf{Y}^{(K)}$  following the bag-of-patches model in (5) with unknown parameters  $\mathbf{f}$ ,  $\mathbf{v}^{(k)}$ , and  $\mathbf{C}^{(k)}$  for  $k = 1, \dots, K$ , our goal is to obtain the foreground material signature  $\mathbf{f}$ . To this end, we regard this problem as an estimation problem wherein  $\mathbf{f}$  is the desired parameter and  $\mathbf{v}^{(k)}$ , and  $\mathbf{C}^{(k)}$  for  $k = 1, \dots, K$  are the nuisance parameters.

**A Key Challenge — Ambiguity in the Bag-of-Patches Model:** As previously identified, the factorization in the bag-of-patches model (5) is not unique. Consider the application of a transformation matrix  $\mathbf{T} = \begin{bmatrix} \alpha & \gamma \\ \beta & \delta \end{bmatrix}$  to each patch  $\mathbf{Y}^{(k)}$  in the model:

$$\begin{aligned} \mathbf{Y}^{(k)} &= \text{diag}(\mathbf{v}^{(k)}) [\mathbf{f} \ \mathbf{1}] \mathbf{T} \mathbf{T}^{-1} \mathbf{C}^{(k)} \\ &= \text{diag}(\tilde{\mathbf{v}}^{(k)}) [\tilde{\mathbf{f}} \ \mathbf{1}] \tilde{\mathbf{C}}^{(k)}, \\ \tilde{\mathbf{v}}^{(k)} &= (\gamma \mathbf{f} + \delta \mathbf{1}) \odot \mathbf{v}^{(k)}, \\ \tilde{\mathbf{C}}^{(k)} &= \mathbf{T}^{-1} \mathbf{C}^{(k)}, \quad \tilde{\mathbf{f}} = (\alpha \mathbf{f} + \beta \mathbf{1}) \oslash (\gamma \mathbf{f} + \delta \mathbf{1}). \end{aligned} \quad (6)$$

The alternative factorization must still respect the properties of the model: the alternative signatures  $\tilde{\mathbf{f}}$  and  $\tilde{\mathbf{v}}^{(k)}$  must be strictly positive, and the coefficient matrices  $\tilde{\mathbf{C}}^{(k)}$  must be non-negative. These constraints are dependent on the data in the set of patches, and the intersection of these constraints defines the space of admissible transformations in the model. It is clear that the bag-of-patches model may have multiple representations for a given set of hyperspectral data. This is typical of unmixing problems; as previously noted, in the linear mixing model estimates of the endmember and abundance matrices may be obtained up to variations of scaling and permutation [40], [41]. Similarly, we will focus on determining identifiability conditions for the intimate mixing model, and defining the

<sup>2</sup>We note that with a rank 1 patch  $\mathbf{Y}^{(k)}$ , for any estimate of foreground material signature  $\tilde{\mathbf{f}}$  there exists a pair of vector  $\tilde{\mathbf{v}}^{(k)}$  and matrix  $\tilde{\mathbf{C}}^{(k)}$  such that  $\mathbf{Y}^{(k)} = \text{diag}(\tilde{\mathbf{v}}^{(k)}) [\tilde{\mathbf{f}} \ \mathbf{1}] \tilde{\mathbf{C}}^{(k)}$ , where  $\tilde{\mathbf{v}}^{(k)} > 0$  and  $\tilde{\mathbf{C}}^{(k)} \geq 0$ . Thus, rank 1 patches do not add any additional constraints not introduced by rank 2 patches, and we may ignore the contribution of such patches to the solution.

characteristic variations of the set of identifiable solutions under such conditions.

### III. THEORY

In this section, we prove exact recovery of the original foreground material signature (up to variations of scaling and elementwise inversion) under appropriate identifiability criteria and data conditions in a noiseless setting. The section proceeds as follows. First, we characterize the space of feasible solutions to the bag-of-patches model in terms of feasible foreground material signatures. Next, we propose two identifiability criteria (minimum volume and endpoint fit). We show that solutions satisfying either criterion will be restricted to specific variations. Then, we propose a data condition and show that the combination of an identifiability criterion and the data condition ensures solutions will match the true foreground material signature (up to variations of scaling and elementwise inversion).

#### A. Solution to the Bag-of-Patches Model

Our goal is to obtain a foreground material signature that satisfies the bag-of-patches model (5) for a given set of patches. We refer to an obtained foreground material signature as a solution to the bag-of-patches model. For any solution to the foreground material there must exist a background-illumination signature and a coefficient matrix for each patch satisfying the bag-of-patches model and its constraints.

**Definition 1 (Solution to Bag-of-Patches Model):** Let  $\mathbf{Y}^{(1)}, \dots, \mathbf{Y}^{(K)}$  be a set of patches that satisfies the bag-of-patches model (5). We say that a vector  $\tilde{\mathbf{f}} \in \mathbb{R}_{++}^M$  is a solution to the bag-of-patches model if there exists  $\tilde{\mathbf{v}}^{(k)} \in \mathbb{R}_{++}^M$  and  $\tilde{\mathbf{C}}^{(k)} \in \mathbb{R}_+^{2 \times N_k}$  for  $k = 1, \dots, K$  that satisfy

- (D1:1)  $\mathbf{Y}^{(k)} = \text{diag}(\tilde{\mathbf{v}}^{(k)}) [\tilde{\mathbf{f}} \ \mathbf{1}] \tilde{\mathbf{C}}^{(k)}$ ;
- (D1:2)  $\tilde{\mathbf{f}} > 0$ ;
- (D1:3)  $\tilde{\mathbf{v}}^{(k)} > 0, \forall k$ ;
- (D1:4)  $\tilde{\mathbf{C}}^{(k)} \geq 0, \forall k$ .

#### B. Solution Ambiguity

The true foreground material signature  $\mathbf{f}$  is a solution to the bag-of-patches model (5) under Definition 1, but other solutions may exist. Section II-C suggests that some alternative solutions may have the form  $\tilde{\mathbf{f}} = (\alpha \mathbf{f} + \beta \mathbf{1}) \odot (\gamma \mathbf{f} + \delta \mathbf{1})$ . In fact, if  $\mathbf{1}$ ,  $\mathbf{f}$ , and  $\mathbf{f} \odot \mathbf{f}$  are linearly independent then the entire space of alternative solutions can be characterized by this form. This can be shown by considering an alternative parameterization of two columns from a single patch, and considering the elementwise ratio of these columns to remove the background-illumination vector parameter. Note that the requirement that  $\mathbf{1}$ ,  $\mathbf{f}$ , and  $\mathbf{f} \odot \mathbf{f}$  are linearly independent is nearly always satisfied in practice, as this condition is equivalent to  $\mathbf{f}$  having at least three distinct entries. This result is stated in Property 1.

**Property 1:** Let  $\mathbf{f} \in \mathbb{R}_{++}^M$  be the true foreground material signature for a set of patches  $\mathbf{Y}^{(1)}, \dots, \mathbf{Y}^{(K)}$  satisfying

the bag-of-patches model (5). Any solution  $\tilde{\mathbf{f}} \in \mathbb{R}_{++}^M$  to the bag-of-patches model satisfies

$$\begin{aligned} \tilde{\mathbf{f}} &= (\alpha \mathbf{f} + \beta \mathbf{1}) \odot (\gamma \mathbf{f} + \delta \mathbf{1}), \\ \tilde{\mathbf{v}}^{(k)} &= \epsilon_k (\gamma \mathbf{f} + \delta \mathbf{1}) \odot \mathbf{v}^{(k)}, \text{ for } k = 1, 2, \dots, K, \\ \tilde{\mathbf{C}}^{(k)} &= \frac{1}{\epsilon_k} \begin{bmatrix} \alpha & \gamma \\ \beta & \delta \end{bmatrix}^{-1} \mathbf{C}^{(k)}, \text{ for } k = 1, 2, \dots, K, \end{aligned}$$

for some  $\alpha, \beta, \gamma, \delta \in \mathbb{R}$  such that  $\alpha\delta - \beta\gamma \neq 0$ , some  $\epsilon_k > 0$ , some  $\tilde{\mathbf{v}}^{(k)} \in \mathbb{R}_{++}^M$ , and some  $\tilde{\mathbf{C}}^{(k)} \in \mathbb{R}_+^{2 \times N_k}$  for  $k = 1, 2, \dots, K$ .

Note that for every choice of all strictly positive  $\epsilon_k$  for  $k = 1, 2, \dots, K$ , there is a corresponding parameterization with reversed sign for the parameters  $\alpha, \beta, \gamma$ , and  $\delta$ , and all strictly negative  $\epsilon_k$  for  $k = 1, 2, \dots, K$  that yields identical material signatures and coefficient matrices. Thus, we can safely restrict the parameterization of the solution to the case of all positive  $\epsilon_k$ .

Property 1 shows that any solution to the bag-of-patches model may be parameterized by coefficients  $\alpha, \beta, \gamma, \delta \in \mathbb{R}$ ,  $\epsilon_k > 0$  for  $k = 1, 2, \dots, K$ , and the true model parameters  $\mathbf{f}$  and  $\mathbf{v}^{(k)}, \mathbf{C}^{(k)}$  for  $k = 1, 2, \dots, K$ . The illumination-background vectors  $\tilde{\mathbf{v}}^{(k)}$  and coefficient matrices  $\tilde{\mathbf{C}}^{(k)}$  are nuisance parameters. We seek to express the space of solutions for the foreground signature independent of the background-illumination vectors and coefficient matrices. Dependence on the true illumination-background vectors can be removed by substituting the definitions of these parameters from Property 1 in the conditions for a solution given in Definition 1. The resulting characterization of a solution is given in the following proposition:

**Proposition 1:** Let  $\mathbf{Y}^{(1)}, \dots, \mathbf{Y}^{(K)}$  be a set of patches that satisfies the bag-of-patches model (5) with a true foreground material signature  $\mathbf{f} \in \mathbb{R}_{++}^M$  and true coefficient matrices  $\mathbf{C} \in \mathbb{R}_+^{2 \times N_k}$  for  $k = 1, \dots, K$ . A vector  $\tilde{\mathbf{f}} \in \mathbb{R}_{++}^M$  is a solution to the bag-of-patches model according to Definition 1 if and only if there exist  $\alpha, \beta, \gamma, \delta \in \mathbb{R}$  such that

- (P1:1)  $\tilde{\mathbf{f}} = (\alpha \mathbf{f} + \beta \mathbf{1}) \odot (\gamma \mathbf{f} + \delta \mathbf{1})$ ;
- (P1:2)  $\alpha \mathbf{f} + \beta \mathbf{1} > 0$ ;
- (P1:3)  $\gamma \mathbf{f} + \delta \mathbf{1} > 0$ ;
- (P1:4)  $\begin{bmatrix} \alpha & \gamma \\ \beta & \delta \end{bmatrix}^{-1} \mathbf{C}^{(k)} \geq 0$ , for  $k = 1, 2, \dots, K$ ;
- (P1:5)  $\alpha\delta - \beta\gamma \neq 0$ .

It is further possible to replace the multiple per-patch constraints in P1:4 with a single constraint; consider the following lemma:

**Lemma 1:** Let  $\mathbf{C}^{(k)} \in \mathbb{R}_+^{2 \times N_k}$  for  $k = 1, \dots, K$  be non-negative matrices where no column is equal to the zero vector and at least one matrix is full row-rank. Define  $r_a$  and  $r_b$  as

$$r_a := \min_{j,k} c_{2,j}^{(k)} / c_{1,j}^{(k)} \quad \text{and} \quad r_b := \min_{j,k} c_{1,j}^{(k)} / c_{2,j}^{(k)}. \quad (7)$$

For coefficients  $\alpha, \beta, \gamma, \delta \in \mathbb{R}$  such that  $\alpha\delta - \beta\gamma \neq 0$ , it holds that

$$\begin{bmatrix} \alpha & \gamma \\ \beta & \delta \end{bmatrix}^{-1} \mathbf{C}^{(k)} \geq 0, \quad \forall k \iff \begin{bmatrix} \alpha & \gamma \\ \beta & \delta \end{bmatrix}^{-1} \begin{bmatrix} 1 & r_b \\ r_a & 1 \end{bmatrix} \geq 0.$$

The proof of Lemma 1 is given in Appendix C. This lemma naturally leads to the following corollary:

**Corollary 1:** Let  $\mathbf{Y}^{(1)}, \dots, \mathbf{Y}^{(K)}$  be a set of patches that satisfies the bag-of-patches model (5) with a true foreground material signature  $\mathbf{f} \in \mathbb{R}_{++}^M$  and true coefficient matrices  $\mathbf{C}^{(k)} \in \mathbb{R}_{++}^{2 \times N_k}$  for  $k = 1, 2, \dots, K$ . Define  $r_a$  and  $r_b$  as in (7). A vector  $\tilde{\mathbf{f}} \in \mathbb{R}_{++}^M$  is a solution to the bag-of-patches model if and only if there exist  $\alpha, \beta, \gamma, \delta \in \mathbb{R}$  such that

$$(C1:1) \quad \tilde{\mathbf{f}} = (\alpha \mathbf{f} + \beta \mathbf{1}) \odot (\gamma \mathbf{f} + \delta \mathbf{1});$$

$$(C1:2) \quad \alpha \mathbf{f} + \beta \mathbf{1} > 0;$$

$$(C1:3) \quad \gamma \mathbf{f} + \delta \mathbf{1} > 0; \text{ and}$$

$$(C1:4) \quad \begin{bmatrix} \alpha & \gamma \\ \beta & \delta \end{bmatrix}^{-1} \begin{bmatrix} 1 & r_b \\ r_a & 1 \end{bmatrix} \geq 0;$$

$$(C1:5) \quad \alpha\delta - \beta\gamma \neq 0.$$

We have formally defined the set of feasible solutions under the bag-of-patches model in Definition 1, and derived a simplified representation of this set in terms of only the foreground material signature in Corollary 1. The set of feasible solutions includes many nonlinear variations of the true foreground material signature, which is difficult to consider for tasks such as foreground material identification or characterization. To address this challenge, we seek conditions and solution criteria under which a set of solutions with a simpler variations may be obtained.

### C. Restricting the Solution Space via Identifiability Criteria

Corollary 1 suggests a space of feasible solutions to the bag-of-patches model (5) with many nonlinear variations. We seek a smaller set of feasible solutions with simpler variations, as in identifiable solutions under the linear mixing model. To achieve this, we first explore restricting the solution space by requiring solutions to satisfy additional criteria. We will introduce two potential criteria: the minimum volume criterion, and the endpoint fit criterion. We will show that solutions satisfying either of these criteria are restricted in a manner that will lead to the desired set of solutions if the appropriate identifiability condition is also satisfied.

**Minimum-volume solution:** The first identifiability criterion we introduce is the minimum volume solution. An estimated foreground material signature  $\tilde{\mathbf{f}}$  satisfies this criterion if it is a local minimum of some volume measure  $\text{Vol}(\tilde{\mathbf{f}})$  and satisfies the standard solution constraints. We consider the normalized determinant as our volume measure:

$$\text{Vol}(\tilde{\mathbf{f}}) = \frac{\det([\tilde{\mathbf{f}} \ \mathbf{1}]^T [\tilde{\mathbf{f}} \ \mathbf{1}])}{\|\mathbf{1}\|_2 \|\tilde{\mathbf{f}}\|_2} = 1 - \left( \frac{(\tilde{\mathbf{f}}^T \mathbf{1})}{\|\mathbf{1}\|_2 \|\tilde{\mathbf{f}}\|_2} \right)^2. \quad (8)$$

Using this volume measure, a minimum-volume solution is described in Definition 2.

**Definition 2 (Minimum-Volume Solution):** Let  $\mathbf{Y}^{(1)}, \dots, \mathbf{Y}^{(K)}$  be a set of patches that satisfies the bag-of-patches model (5). A vector  $\mathbf{f}^* \in \mathbb{R}_{++}^M$  is a minimum-volume solution to the bag-of-patches model if  $\mathbf{f}^*$  is a local minimizer of (8) subject to the constraints in Definition 1 (or equivalently in Corollary 1).

A simple characterization of minimum-volume solutions to the bag-of-patches model (5) can be obtained in terms of a

unique element of the feasible space described in Property 1, denoted by  $\mathbf{f}_0$  and defined as

$$\mathbf{f}_0 = (\mathbf{f} + r_a \mathbf{1}) \odot (r_b \mathbf{f} + \mathbf{1}), \quad (9)$$

where  $r_a$  and  $r_b$  are defined as in Lemma 1.

**Theorem 1:** Let  $\mathbf{Y}^{(1)}, \dots, \mathbf{Y}^{(K)}$  be a set of patches that satisfies the bag-of-patches model (5) with a true foreground material signature  $\mathbf{f} \in \mathbb{R}_{++}^M$  and true coefficient matrices  $\mathbf{C}^{(k)} \in \mathbb{R}_{++}^{2 \times N_k}$  for  $k = 1, 2, \dots, K$ . Define  $\text{Vol}(\tilde{\mathbf{f}})$  as in (8). Let  $\mathbf{f}_0$  be defined as in (9). A solution  $\mathbf{f}^* \in \mathbb{R}_{++}^M$  to the bag-of-patches model is a minimum-volume solution if and only if

$$\mathbf{f}^* = c \mathbf{f}_0 \quad \text{or} \quad \mathbf{f}^* = c \mathbf{1} \odot \mathbf{f}_0, \quad c > 0. \quad (10)$$

The proof of Theorem 1 is given in Appendix A. Note that the variations present in minimum-volume solutions are scaling and element-wise inversion; this is similar to the variations for identifiable solutions to the NMF problem. In particular, element-wise inversion may be viewed as the result of permuting the position of endmember estimates  $\tilde{\mathbf{v}} \odot \tilde{\mathbf{f}}$  and  $\tilde{\mathbf{v}}$  when computing the ratio to obtain  $\tilde{\mathbf{f}}$ .

**End-point solution:** The second identifiability criterion we introduce is the endpoint fit solution. For a given factorization under the bag-of-patches model, we observe that the columns of a coefficient matrix  $\mathbf{C}^{(k)}$  suggest a notion of coordinates for a given pixel in terms of  $\mathbf{v}^{(k)} \odot \mathbf{f}$  and  $\mathbf{v}^{(k)}$ . The space of valid coordinates is constrained by the non-negativity requirement for coefficients. Consider a coefficient column with one of the following forms:  $[x, 0]^T$ , or  $[0, y]^T$ , where  $x$  and  $y$  are positive constants. Any pixel with such a form of coordinates lies at the edge of the coordinate space. We refer to such a pixel as an *endpoint*. A solution  $\tilde{\mathbf{f}}$  satisfies the endpoint fit criterion if, for the corresponding factorization under the bag-of-patches model, there exists at least one of each form of endpoint. The definition follows:

**Definition 3 (Endpoint Fit Solution):** Let  $\mathbf{Y}^{(1)}, \dots, \mathbf{Y}^{(K)}$  be a set of patches that satisfies the bag-of-patches model (5) with a true foreground material signature  $\mathbf{f} \in \mathbb{R}_{++}^M$  and true coefficient matrices  $\mathbf{C}^{(k)} \in \mathbb{R}_{++}^{2 \times N_k}$  for  $k = 1, 2, \dots, K$ . A solution  $\mathbf{f}^*$  to the bag-of-patches model is an endpoint fit solution if there exist estimated coefficient matrices  $\tilde{\mathbf{C}}^{(k)}$  for  $k = 1, 2, \dots, K$  such that  $\tilde{\mathbf{C}}^{(k)}$  contains a column  $[x, 0]^T$  for some  $k = k_1$ , and contains a column  $[0, y]^T$  for some  $k = k_2$ , where  $x, y > 0$ .<sup>3</sup>

Similar to minimum-volume solutions, endpoint fit solutions to the bag-of-patches model (5) may be stated in terms of  $\mathbf{f}_0$ . The nature of endpoint fit solutions is characterized in the following theorem.

**Theorem 2:** Let  $\mathbf{Y}^{(1)}, \dots, \mathbf{Y}^{(K)}$  be a set of patches that satisfies the bag-of-patches model (5) with a true foreground material signature  $\mathbf{f} \in \mathbb{R}_{++}^M$  and true coefficient matrices  $\mathbf{C}^{(k)} \in \mathbb{R}_{++}^{2 \times N_k}$  for  $k = 1, \dots, K$ . Let  $\mathbf{f}_0$  be defined as in (9). A solution  $\mathbf{f}^*$  to the bag-of-patches model is an endpoint fit solution if and only if

$$\mathbf{f}^* = c \mathbf{f}_0 \quad \text{or} \quad \mathbf{f}^* = c \mathbf{1} \odot \mathbf{f}_0, \quad c > 0. \quad (11)$$

<sup>3</sup>The indices  $k_1$  and  $k_2$  need not be distinct. In such a case, both kinds of endpoint occur in the same estimated coefficient matrix.



The proof of Theorem 2 is given in Appendix B.

A corollary of Theorem 1 and Theorem 2 is that minimum-volume solutions and endpoint fit solutions are equivalent:

*Corollary 2:* Let  $\mathbf{Y}^{(1)}, \dots, \mathbf{Y}^{(K)}$  be a set of patches that satisfies the bag-of-patches model (5). A solution  $\mathbf{f}^* \in \mathbb{R}_{++}^M$  to the bag-of-patches model is a minimum-volume solution if and only if it is an endpoint fit solution.

According to Corollary 2, every minimum-volume solution is an endpoint fit solution, and vice versa. We will use this result later in developing an algorithm to identify an endpoint fit solution.

#### D. Complete Solutions With Identifiability Conditions

Although minimum volume and endpoint fit criteria offer a unique solution up to the variations of scaling and element-wise inversion of  $\mathbf{f}_0$ , they are not guaranteed to recover the true foreground material signature  $\mathbf{f}$ . If and only if  $r_a = r_b = 0$  then  $\mathbf{f}_0 = \mathbf{f}$ . From the definition of  $r_a$  and  $r_b$  in (7), this implies that there must exist columns among all the coefficient matrices  $\mathbf{C}^{(k)}$  for  $k = 1, \dots, K$  of the form  $[\alpha, 0]^T$  and  $[0, \beta]^T$ , where  $\alpha, \beta > 0$ . This data condition is stated formally in the following definition:

*Definition 4 (Full-tightness):* Let  $\mathbf{Y}^{(1)}, \dots, \mathbf{Y}^{(K)}$  be a set of patches that satisfies the bag-of-patches model (5) with a true foreground material signature  $\mathbf{f} \in \mathbb{R}_{++}^M$  and true coefficient matrices  $\mathbf{C} \in \mathbb{R}_{++}^{2 \times N_k}$  for  $k = 1, \dots, K$ . Suppose there exists a patch  $\mathbf{Y}^{(k_1)}$  containing a scaled version of  $\mathbf{v}^{(k_1)} \odot \mathbf{f}$  and a patch  $\mathbf{Y}^{(k_2)}$  containing a scaled version of  $\mathbf{v}^{(k_2)}$ . Note that we do not require  $k_1$  and  $k_2$  to be distinct. Equivalently, there exists a column  $[\alpha, 0]^T$  in  $\mathbf{C}^{(k_1)}$  and a column  $[0, \beta]^T$  in  $\mathbf{C}^{(k_2)}$  with  $\alpha, \beta > 0$  (this implies  $r_a = r_b = 0$ ). We say that such a set of patches is fully tight with respect to  $\mathbf{f}$ .

The full-tightness condition in Definition 4, coupled with the minimum volume solution criterion in Definition 2 and/or the endpoint fit solution criterion in Definition 3, ensure that solutions match the true foreground material signature up to variations of scaling and element-wise inversion. We state this result in Theorem 3.

*Theorem 3:* Let  $\mathbf{Y}^{(1)}, \dots, \mathbf{Y}^{(K)}$  be a set of patches that satisfies the bag-of-patches model (5) with a true foreground material signature  $\mathbf{f} \in \mathbb{R}_{++}^M$  and true coefficient matrices  $\mathbf{C} \in \mathbb{R}_{++}^{2 \times N_k}$  for  $k = 1, \dots, K$ . If  $\mathbf{f}^*$  is either a minimum-volume solution or an endpoint fit solution to the bag-of-patches model, and the set of patches is fully tight with respect to  $\mathbf{f}$ , then

$$\mathbf{f}^* = c\mathbf{f} \text{ or } \mathbf{f}^* = c\mathbf{1} \odot \mathbf{f}, \quad c > 0.$$

In conclusion, any minimum-volume solution or endpoint fit solution will belong to the identifiable set of solutions if the set of patches satisfies the full-tightness condition.

## IV. ALGORITHMS

In the previous section, we proposed two criteria under which identifiable solutions to the foreground material signature extraction problem may be found: a minimum volume solution and an endpoint fit solution. In this section, we propose two

algorithms to solve the foreground material signature extraction problem based on these criteria. First, we consider a projected block coordinate descent algorithm with volume regularization to find solutions satisfying the minimum volume criterion. Then, we adapt the projected block coordinate descent algorithm *without* regularization to instead find solutions satisfying the endpoint fit criterion.

#### A. Finding Minimum Volume Solutions

The first approach we consider is to find an estimated foreground material signature that satisfies the minimum volume criterion. According to Definition 2, such a solution must be a local minimum of the volume measure  $\text{vol}(\tilde{\mathbf{f}})$  in (8) subject to the constraints D1:1-D1:4. The constraints in D1:2 and D1:3 are strict inequalities, which are difficult to consider for optimization. We consider a relaxation of these constraints to be non-strict. It can be shown that any parameters  $\tilde{\mathbf{f}}$  and  $\tilde{\mathbf{v}}^{(k)}$  for  $k = 1, 2, \dots, K$  satisfying the minimum volume criterion under non-strict inequality constraints must be strictly positive. Thus, minimum volume solutions under relaxed constraints are also minimum volume solutions under strict constraints.

The exact fitting constraint in D1:1 is also challenging from an optimization perspective. Instead, we take the approach of previous works [42], [43], [44] and reformulate the objective as

$$\begin{aligned} g(\tilde{\mathbf{f}}, \tilde{\mathbf{v}}^{(1)}, \dots, \tilde{\mathbf{v}}^{(K)}, \tilde{\mathbf{C}}^{(1)}, \dots, \tilde{\mathbf{C}}^{(K)}) \\ = \sum_{k=1}^K \|\mathbf{Y}^{(k)} - \text{diag}(\tilde{\mathbf{v}}^{(k)}) [\tilde{\mathbf{f}} \mathbf{1}] \tilde{\mathbf{C}}^{(k)}\|_F^2 + \lambda \text{Vol}(\tilde{\mathbf{f}}), \end{aligned} \quad (12)$$

where  $\lambda$  is a positive regularization weight that determines the significance of the volume measure in the optimization problem. To obtain a unique solution, we consider an equality constraint for the norms of  $\tilde{\mathbf{f}}$  and  $\tilde{\mathbf{v}}^{(k)}$  for  $k = 1, 2, \dots, K$ . Using regularization and the considered constraints, an optimization problem corresponding to a minimum-volume solution is

$$\begin{aligned} \min \quad & g(\tilde{\mathbf{f}}, \tilde{\mathbf{v}}^{(1)}, \dots, \tilde{\mathbf{v}}^{(K)}, \tilde{\mathbf{C}}^{(1)}, \dots, \tilde{\mathbf{C}}^{(K)}) \\ \text{s.t.} \quad & \tilde{\mathbf{f}} \geq 0, \|\tilde{\mathbf{f}}\| = 1, \\ & \tilde{\mathbf{v}}^{(k)} \geq 0, \|\tilde{\mathbf{v}}^{(k)}\| = 1, \text{ for } k = 1, 2, \dots, K, \\ & \tilde{\mathbf{C}}^{(k)} \geq 0, \text{ for } k = 1, 2, \dots, K. \end{aligned} \quad (13)$$

The minimization problem is separable with respect to each estimated background-illumination signature  $\tilde{\mathbf{v}}^{(k)}$  and estimated coefficient matrix  $\tilde{\mathbf{C}}^{(k)}$  for  $k = 1, 2, \dots, K$ . Additionally, the minimization problem for each of these terms depends only on the fitting error of the corresponding patch  $\mathbf{Y}^{(k)}$ . Note that the problem is not separable with respect to  $\tilde{\mathbf{f}}$ . This suggests an approach based on projected block coordinate descent. We refer to our algorithm based on this approach as MinVolFit. The algorithm is listed in Algorithm 1. Let  $N$  be the number of pixels distributed among all patches; the per-iteration complexity of this algorithm is  $O(MN)$ . For details on computation

**Algorithm 1** MinVolFit: find a solution to (13).

---

**Input:**  $\mathcal{Y} = \{\mathbf{Y}^{(1)}, \dots, \mathbf{Y}^{(K)}\}$ ,  $\lambda$ ,  $N_{\text{iters}}$

**for**  $k = 1, 2, \dots, K$  **do**

Randomly initialize  $\mathbf{v}_0^{(k)} \in \mathbb{R}_{++}^M$  and  $\mathbf{C}_0^{(k)} \in \mathbb{R}_{++}^{M \times N_k}$

**end for**

Randomly initialize  $\mathbf{f}_0 \in \mathbb{R}_{++}^M$

Define  $f_k(\cdot) = \left\| \mathbf{Y}^{(k)} - \text{diag}(\mathbf{v}^{(k)})[\mathbf{f}_{k+1}] \mathbf{C}^{(k)} \right\|_F^2$

Define  $g(\cdot) = \sum_{k=1}^K f_k(\cdot) + \lambda \mathbf{f}$

**for**  $j = 1, \dots, N_{\text{iters}}$  **do**

In each step, select  $\eta$  appropriately via backtracking

**for**  $k = 1, 2, \dots, K$  **do**

$\mathbf{C}_j^{(k)} \leftarrow P_+ \left( \mathbf{C}_{j-1}^{(k)} - \eta \left( \nabla_{\mathbf{C}^{(k)}} f_k(\cdot) \right) \Big|_{\mathbf{v}_{j-1}^{(k)}, \mathbf{C}_{j-1}^{(k)}} \right)$

%  $P_+$  is the projection onto the non-negative orthant

$\mathbf{v}_j^{(k)} \leftarrow P_{U_+} \left( \mathbf{v}_{j-1}^{(k)} - \eta \left( \nabla_{\mathbf{v}^{(k)}} f_k(\cdot) \right) \Big|_{\mathbf{v}_{j-1}^{(k)}, \mathbf{C}_j^{(k)}} \right)$

%  $P_{U_+}$  is the projection onto the intersection of the non-negative orthant and the surface of the unit sphere

**end for**

$\mathbf{f}_j \leftarrow P_{U_+} \left( \mathbf{f}_{j-1} - \eta \left( \nabla_{\mathbf{f}} g(\cdot) \right) \Big|_{\mathbf{f}_{j-1}, \mathbf{v}_j^{(k)}, \mathbf{C}_j^{(k)}, \forall k} \right)$

**end for**

**return**  $\mathbf{f}_{N_{\text{iters}}}, \mathbf{v}_{N_{\text{iters}}}^{(1)}, \dots, \mathbf{v}_{N_{\text{iters}}}^{(K)}, \mathbf{C}_{N_{\text{iters}}}^{(1)}, \dots, \mathbf{C}_{N_{\text{iters}}}^{(K)}$

---

complexity and the projection onto the intersection of the non-negative orthant and the surface of the unit sphere, we refer the reader to the supplementary material.

### B. Finding Endpoint Fit Solutions

Selecting an optimal regularization weight  $\lambda$  is not trivial, and experimental results show that the accuracy of the estimated foreground material signature is very sensitive to the choice of hyperparameter. We seek an alternative method that is less sensitive to the choice of hyperparameter. The next algorithmic approach we consider is to find a foreground material signature that satisfies the endpoint fit criterion (see Definition 3). Consider the following lemma:

**Lemma 2:** Let  $\mathbf{Y}^{(1)}, \dots, \mathbf{Y}^{(K)}$  be a set of patches generated according to the bag-of-patches model (5). Suppose there exist element-wise positive vectors  $\mathbf{d}_1, \dots, \mathbf{d}_K$  such that the rank of the concatenated matrix  $[\text{diag}(\mathbf{d}_1)\mathbf{Y}^{(1)}, \dots, \text{diag}(\mathbf{d}_K)\mathbf{Y}^{(K)}]$  is exactly 2:

$$\text{rank}\{[\text{diag}(\mathbf{d}_1)\mathbf{Y}^{(1)} \quad \dots \quad \text{diag}(\mathbf{d}_K)\mathbf{Y}^{(K)}]\} = 2.$$

If  $\tilde{\mathbf{y}}_i$  and  $\tilde{\mathbf{y}}_j$  are distinct columns from the matrix  $[\text{diag}(\mathbf{d}_1)\mathbf{Y}^{(1)} \quad \dots \quad \text{diag}(\mathbf{d}_K)\mathbf{Y}^{(K)}]$  that maximize

$$\tilde{\mathbf{y}}_i^T \tilde{\mathbf{y}}_j / (\|\tilde{\mathbf{y}}_i\|_2 \|\tilde{\mathbf{y}}_j\|_2), \quad (14)$$

then  $\mathbf{f}^* = \tilde{\mathbf{y}}_i \odot \tilde{\mathbf{y}}_j$  is an endpoint fit solution for the set of patches  $\mathbf{Y}^{(1)}, \dots, \mathbf{Y}^{(K)}$ .

The proof is given in the supplementary material. In the noiseless case, MinVolFit with  $\lambda=0$  produces a factorization of a set of patches such that the  $k$ th patch lies in the non-negative span of  $\tilde{\mathbf{v}}^{(k)} \odot \mathbf{f}$  and  $\tilde{\mathbf{v}}^{(k)}$  for  $k = 1, 2, \dots, K$ . Noting that each  $\tilde{\mathbf{v}}^{(k)}$  will be strictly positive, we

**Algorithm 2** EPFit: find a solution to the bag-of-patches model (5) satisfying the endpoint fit criterion.

---

**Input:**  $\mathcal{Y} = \{\mathbf{Y}^{(1)}, \dots, \mathbf{Y}^{(K)}\}$

$\tilde{\mathbf{v}}^{(1)}, \dots, \tilde{\mathbf{v}}^{(K)} \leftarrow \text{MinVolFit}(\mathcal{Y}, \lambda=0)$

$\tilde{\mathbf{Y}} \leftarrow [\text{diag}(\tilde{\mathbf{v}}^{(1)})^{-1}\mathbf{Y}^{(1)} \quad \dots \quad \text{diag}(\tilde{\mathbf{v}}^{(K)})^{-1}\mathbf{Y}^{(K)}]$

$\mathbf{u}_1, \mathbf{u}_2 \leftarrow \tilde{\mathbf{y}}_1, \tilde{\mathbf{y}}_2$

**for**  $n = 3, 4, \dots, N$  **do**

$\mathbf{w} \leftarrow \tilde{\mathbf{y}}_n$

**if**  $\mathbf{u}_1^T \mathbf{w} / (\|\mathbf{u}_1\|_2 \|\mathbf{w}\|_2) > \mathbf{u}_1^T \mathbf{u}_2 / (\|\mathbf{u}_1\|_2 \|\mathbf{u}_2\|_2)$  **then**

$\mathbf{u}_2 \leftarrow \mathbf{w}$

**else if**  $\mathbf{w}^T \mathbf{u}_2 / (\|\mathbf{w}\|_2 \|\mathbf{u}_2\|_2) > \mathbf{u}_1^T \mathbf{u}_2 / (\|\mathbf{u}_1\|_2 \|\mathbf{u}_2\|_2)$  **then**

$\mathbf{u}_1 \leftarrow \mathbf{w}$

**end if**

**end for**

$\mathbf{f}^* \leftarrow \mathbf{u}_1 \odot \mathbf{u}_2$

**return**  $\mathbf{f}^*$

---

have  $\text{diag}(\tilde{\mathbf{v}}^{(k)})^{-1}\mathbf{Y}^{(k)} = [\tilde{\mathbf{f}} \quad \mathbf{1}] \tilde{\mathbf{C}}^{(k)}$ . Concatenating across all patches for  $k = 1, 2, \dots, K$  yields

$$\begin{aligned} & [\text{diag}(\tilde{\mathbf{v}}^{(1)})^{-1}\mathbf{Y}^{(1)} \quad \dots \quad \text{diag}(\tilde{\mathbf{v}}^{(K)})^{-1}\mathbf{Y}^{(K)}] \\ &= [\tilde{\mathbf{f}} \quad \mathbf{1}] [\tilde{\mathbf{C}}^{(1)} \quad \dots \quad \tilde{\mathbf{C}}^{(K)}]. \end{aligned} \quad (15)$$

This follows the form of Lemma 2, so an endpoint fit solution is given by the columns of the left matrix that maximize the normalized inner product in (14). If patches contain random noise, then each matrix  $\text{diag}(\tilde{\mathbf{v}}^{(k)})^{-1}\mathbf{Y}^{(k)}$  lies approximately in the non-negative span of  $\tilde{\mathbf{f}}$  and  $\mathbf{1}$ , and the endpoint fit solution suggested by Lemma 2 is an approximate solution. The algorithm is listed in Algorithm 2. Let  $N$  be the number of pixels distributed among all patches. Similar to MinVolFit, the per-iteration complexity of EPFit is  $O(MN)$ . For details on computation complexity, we refer the reader to the supplementary material.

## V. EXPERIMENTS

Our experiments are intended to provide empirical verification of our algorithms in comparison to benchmark approaches in a variety of settings. We consider synthetic data experiments to demonstrate the effectiveness of our algorithms in response to particular choices of SNR and data distribution.

### A. Synthetic Data Experiments

We present synthetic data experiments to verify that our proposed algorithms can identify foreground material signatures with lower error than benchmark approaches; to demonstrate the effectiveness of each proposed algorithm as a function of signal-to-noise ratio (SNR); and to show the effect of different data modeling assumptions on the accuracy of all methods. We will show that our algorithms, which can adapt to varying backgrounds per patch, will obtain more accurate foreground material signature estimates than a benchmark algorithm which does not account for varying backgrounds. We will show that the EPFit algorithm (implemented based on Section IV-B) will show an inverse relationship between SNR and the spectral angular



**Algorithm 3** Generate data for synthetic experiments.

---

**Input:**  $K, M, N, r, p, \sigma^2, \text{is\_strict}$   
 Sample  $\mathbf{f} \sim U\{[0.5, 1.5]\}^M$  and  $\mathbf{v}_{\text{shared}} \sim U\{[0.5, 1.5]\}^M$   
**for**  $k = 1, \dots, K$  **do**  
   Sample  $\mathbf{v}_{\text{individual}}^{(k)} \sim U\{[-0.5, 0.5]\}^M$   
    $\mathbf{v}^{(k)} \leftarrow \mathbf{v}_{\text{shared}} + r \cdot \mathbf{v}_{\text{individual}}^{(k)}$   
   Sample  $q, s \sim U\{[0, 1]\}$   
   **if**  $q \geq p$  and **is\\_strict** **then**  
     % *strictly tight patch*  
     Sample  $\boldsymbol{\theta} \sim U\{[0, \pi/2]\}^N$  and set  $\theta_1 \leftarrow 0$  and  $\theta_2 \leftarrow \pi/2$   
     **else if**  $q \geq p$  and not **is\\_strict** and  $s \geq 0.5$  **then**  
       % *partially tight patch (includes  $\mathbf{b}$  vector)*  
       Sample  $\boldsymbol{\theta} \sim U\{[\pi/8, \pi/2]\}^N$  and set  $\theta_1 \leftarrow \pi/2$   
     **else if**  $q \geq p$  and not **is\\_strict** and  $s < 0.5$  **then**  
       % *partially tight patch (includes  $\mathbf{b} \odot \mathbf{f}$  vector)*  
       Sample  $\boldsymbol{\theta} \sim U\{[0, 3\pi/8]\}^N$  and set  $\theta_1 \leftarrow 0$   
     **else**  
       % *non-tight patch*  
       Sample  $\boldsymbol{\theta} \sim U\{[\pi/8, 3\pi/8]\}^N$   
   **end if**  
   Sample  $r_{\min} \sim U\{[0.5, 1]\}$  and  $r_{\max} \sim U\{[1, 1.5]\}$   
   Sample  $\mathbf{r} \sim U\{[r_{\min}, r_{\max}]\}^N$   
    $\mathbf{C}^{(k)} \leftarrow \begin{bmatrix} \mathbf{r}^T \odot \cos(\boldsymbol{\theta}^T) \\ \mathbf{r}^T \odot \sin(\boldsymbol{\theta}^T) \end{bmatrix}$   
   Sample  $\mathbf{V} \in \mathbb{R}^{M \times N}$  with  $V_{ij} \sim \mathcal{N}(0, \sigma^2), \forall i, j$   
    $\mathbf{Y}^{(k)} \leftarrow (\text{diag}(\mathbf{v}^{(k)})[\mathbf{f} \& 1] \mathbf{C}^{(k)} + \mathbf{V})_+$   
**end for**  
**return**  $\mathbf{Y}^{(k)}, \mathbf{v}^{(k)}, \mathbf{C}^{(k)}$  for  $k = 1, \dots, K$ , and  $\mathbf{f}$

---

difference (SAD) between the estimated and true foreground material signatures. For the MinVolFit algorithm (implemented based on Section IV-A), we will show that for each value of SNR there exists an appropriate choice of regularization weight that will minimize the SAD. Finally, we will show that the MinVolFit algorithm will show a higher resilience to noise than the EPfit algorithm.

**Data generation:** To facilitate synthetic data experiments, we generate sets of patches with a single foreground material signature  $\mathbf{f}$  and several background-illumination vectors  $\mathbf{v}^{(1)}, \dots, \mathbf{v}^{(K)}$ . The exact process of generating data is described in Algorithm 3. The parameters of this algorithm are: ( $K$ ) number of patches to generate, ( $N$ ) number of pixels per patch, ( $M$ ) number of entries per pixel, ( $r$ ) weight coefficient for similarity of background-illumination vectors, ( $p$ ) probability of *tight* patch, ( $\sigma^2$ ) variance of random Gaussian noise, (**is\\_strict**) use *strictly tight* or *partially tight* patch setting. In the *strictly tight* patch setting, tight patches contain one pixel proportional to  $\mathbf{v}^{(k)}$  and another pixel proportional to  $\mathbf{v}^{(k)} \odot \mathbf{f}$ . In the *partially tight* patch setting, tight patches contain one pixel proportional to either  $\mathbf{v}^{(k)}$  or  $\mathbf{v}^{(k)} \odot \mathbf{f}$  and not both. The outputs of the data generation procedure are the patches  $\mathbf{Y}^{(k)}$ , ground truth background-illumination vectors  $\mathbf{v}^{(k)}$ , and ground truth coefficient matrices  $\mathbf{C}^{(k)}$  for  $k = 1, \dots, K$ , and the ground truth foreground material signature  $\mathbf{f}$ .

**Algorithms:** For our experiments, we consider our two proposed methods and three benchmark algorithms: an adapted version of MinVolNMF [18], [45], BMMF-LS-NM [32], and SNPALQ [33]. Given a non-negative input matrix  $\mathbf{Y} \in \mathbb{R}_+^{M \times N}$ ,

MinVolNMF solves the following problem:

$$\begin{aligned} \min \quad & \|\mathbf{Y} - \mathbf{W}\mathbf{H}\|_F^2 + \mu \log \det(\mathbf{W}^T \mathbf{W} + \delta \mathbf{I}) \\ \text{s.t.} \quad & \mathbf{W} \in \mathbb{R}_+^{M \times 2}, \quad \mathbf{H} \in \mathbb{R}_+^{2 \times N}, \end{aligned} \quad (16)$$

where the  $\delta \mathbf{I}$  term for small but sufficiently large  $\delta > 0$  ensures that the determinant is positive. Given a patch following the bag-of-patches model, the NMF problem is equivalent to finding matrices  $\mathbf{W} = [\mathbf{v} \odot \mathbf{f}, \mathbf{v}]$  and  $\mathbf{H} = \mathbf{C}$ . The foreground material signature for the patch can be extracted by taking the element-wise ratio of columns of  $\mathbf{W}$ . Note that volume-minimizing NMF methods allow for permutation and scaling of the recovered columns of  $\mathbf{W}$ . If the correct columns of  $\mathbf{W}$  are identified, then the extracted foreground material signature  $\hat{\mathbf{f}}$  for the patch may be of the form  $\hat{\mathbf{f}} \propto \mathbf{f}$  or  $\hat{\mathbf{f}} \propto \mathbf{1} \odot \mathbf{f}$ . We adapt MinVolNMF to the multiple patch setting by concatenating each patch  $\mathbf{Y}^{(k)}$  for  $k = 1, \dots, K$  such that  $\mathbf{Y}_{\text{all}} = [\mathbf{Y}^{(1)}, \dots, \mathbf{Y}^{(K)}]$ . Then, we apply MinVolNMF to the concatenated matrix. The remaining two benchmark algorithms are adapted to the multiple patch setting similarly, and the foreground signature estimate is chosen post-hoc as the estimated material signature with the smallest SAR measure with respect to the true foreground material signature.

We consider tuning several hyperparameters among the algorithms considered. For the proposed MinVolFit algorithm, we must select a regularization weight and an iteration limit. After initial testing, we selected  $N_{\text{iters}} = 1 \times 10^6$ . We also explore the impact of various choices of regularization weight. For the proposed EPfit algorithm, we must select an iteration limit. We selected  $N_{\text{iters}} = 5 \times 10^4$ . For the MinVolNMF benchmark, we explore several choices of regularization weight. For SNPALQ, we select the number of spectral signatures to estimate as the sum of the number of generated background signatures and the foreground signature.

**Evaluation metric:** As in [44] for endmembers, we evaluate the accuracy of an extracted foreground material signature by measuring the spectral angular difference (SAD) between the estimated and true foreground material signatures. The SAD between two vectors  $\mathbf{u}$  and  $\mathbf{v}$  in degrees is

$$\text{SAD}(\mathbf{u}, \mathbf{v}) = \frac{180}{\pi} \cdot \cos^{-1} \left( \frac{\mathbf{u}^T \mathbf{v}}{\|\mathbf{u}\| \|\mathbf{v}\|} \right). \quad (17)$$

The squared error (SE) measure is also considered in the literature [3], [14]. A typical assumption for the SE measure is that spectral signature estimates are normalized (to accommodate ambiguity of scaling). The SE with normalization measure is defined as  $\text{SE}(\mathbf{u}, \mathbf{v}) := \|\mathbf{u}/\|\mathbf{u}\|_2 - \mathbf{v}/\|\mathbf{v}\|_2\|_2^2$ . We note that the SAD and SE with normalization measure have a one-to-one monotonic relation:

$$\text{SAD}(\mathbf{u}, \mathbf{v}) = 2 \sin^{-1}(\sqrt{\text{SE}(\mathbf{u}, \mathbf{v})/2}) \times \frac{180}{\pi}. \quad (18)$$

Due to the strong similarity of results computed under either the SAD or SE measure, we present results only using the SAD measure for brevity.

<sup>4</sup>This value was selected based on observed convergence of the objective value. In practice, a stopping criterion such as thresholding the minimum change in objective value may be used.

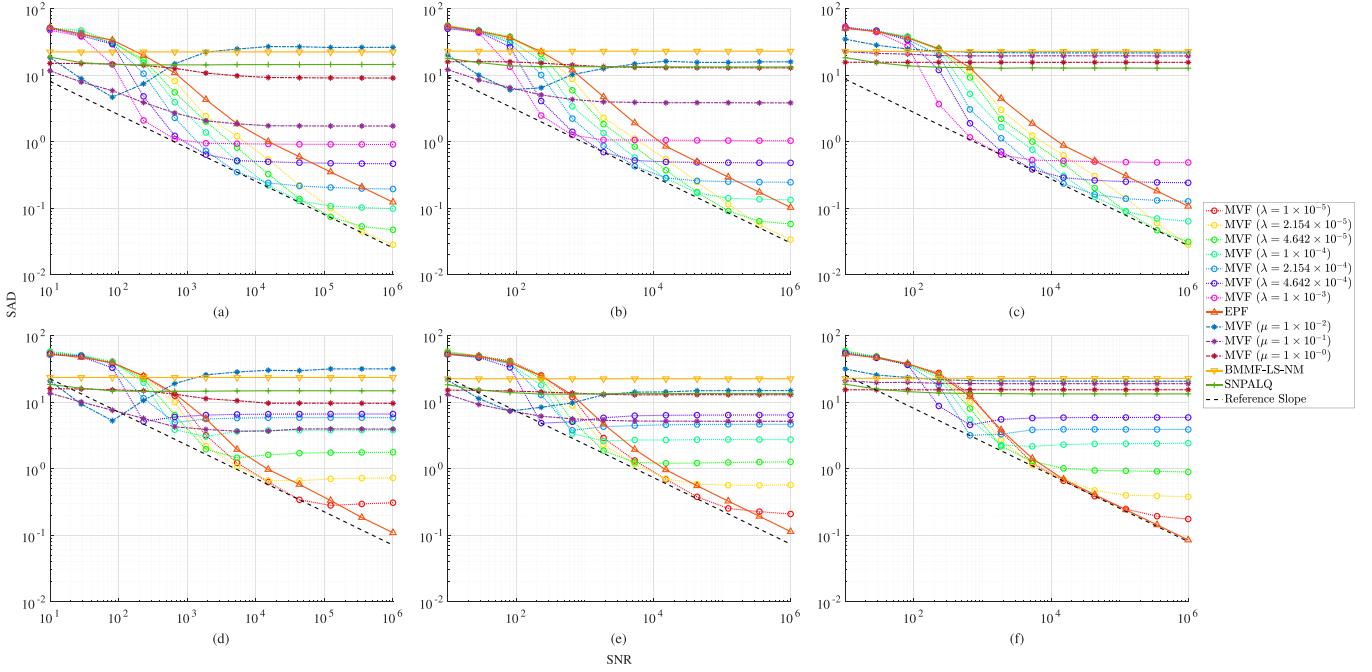


Fig. 2. Plot of mean SAD (measured in degrees) between the estimated and true foreground signatures as a function of SNR for our proposed algorithms and three benchmark algorithms on data generated using (a) strictly-tight patches with low background variation ( $r = 0.1$ ); (b) strictly-tight patches with medium background variation ( $r = 0.2$ ); (c) strictly-tight patches with high background variation ( $r = 1$ ); (d) partially-tight patches with low background variation ( $r = 0.1$ ); (e) partially-tight patches with medium background variation ( $r = 0.2$ ); partially-tight patches with high background variation ( $r = 1$ ). See Section V; data generation for further details. A lower envelope of MinVolFit is shown (black dashed line). Plots for MinVolFit whose curves do not intersect the lower envelope line within the selected range of SNR are omitted.

Our proposed methods and the three benchmark methods can only provide an estimate  $\hat{\mathbf{f}}$  of the true foreground material signature  $\mathbf{f}$  up to the variations of scaling and elementwise inverse. To accommodate these variations, we consider both the normal and elementwise inverse forms of the identified solution as candidates for comparison. The SAD for the standard and inverse forms are given by  $\Delta\theta(\mathbf{f}, \hat{\mathbf{f}})$  and  $\Delta\theta(\mathbf{f}, \mathbf{1} \odot \hat{\mathbf{f}})$ , respectively. We take the minimum of the two measures.

**Results and analysis:** For our experiments, we explore the relation between SNR and the SAD between estimated foreground material signatures and true signatures for all considered algorithms over a range of data generation schemes. We conduct three experiments in a strictly tight patch setting, and three experiments in a partially tight patch setting. For each patch setting, we conduct one experiment each with the following ratios of expected magnitudes for the base and varying background-illumination signature components: low ratio ( $r = 0.1$ ), medium variation ( $r = 0.2$ ), and high ratio ( $r = 1$ ). For each experiment, we consider 10 SNR values logarithmically spaced over the range of  $10^1$  to  $10^6$ . Each value of SNR has a corresponding value of noise variance in the data generation procedure described previously; this value is computed as the ratio of the average squared magnitude of all pixel entries in the data and SNR. For each noise level, we generate a set of 20 bags consisting of 10 patches each as detailed in the data generation section above, with each patch containing 25 pixels of dimension 30. In all cases we use  $p = 0.5$ . To each bag of patches, we apply: MinVolFit with seven values of  $\lambda$

logarithmically spaced between  $1 \times 10^{-5}$  and  $1 \times 10^{-3}$ , EPFit, the adapted MinVolNMF with three values of  $\mu$  logarithmically spaced between  $1 \times 10^{-2}$  and  $1 \times 10^0$  and with the default  $\delta = 0.1$ , BMMF-LS-NM, and SNPALQ. We then compute the SAD between the obtained estimates of the foreground material signature and the true foreground material signature as described in the evaluation metric section above. We report the mean SAD as a function of SNR for each algorithm.

Fig. 2 illustrates the performance of the considered algorithms for both the strictly tight (top row) and partially tight (bottom row) patch settings. For the MinVolFit algorithm, each choice of regularization weight yields a performance curve with decreasing SAD as SNR increases up to some limit in SNR, after which the SAD no longer decreases. As the regularization weight decreases, the SNR value at which the minimum SAD is achieved increases. The lower envelope of performance curves among all choices of regularization weight (depicted by the black line) shows a consistent inverse relationship between SNR and SAD. This may be explained by considering the effect of different choices of regularization weight. In a noisy setting, the noise on endpoints may cause the optimal fit of the foreground material signature with respect to fitting error to have a larger volume relative to the true foreground material signature. Volume regularization allows for an increase in fitting error by rewarding a decrease in volume, so for a given value of SNR there should exist an optimal choice of regularization weight that sufficiently reduces the volume of the estimated foreground material signature. As SNR increases, the effect of

noisy endpoints is reduced and a smaller regularization weight will be optimal. For the EPFit algorithm, in all plots we observe the SAD decreasing as SNR increases.

In contrast to both proposed methods, all three benchmark algorithms demonstrate minimal decrease in SAD as SNR increases. For MinVolNMF, this performance may be explained by considering the effect of a per-patch varying background material signature. MinVolNMF attempts to find a rank-2 NMF representation of the concatenated set of patches, but the varying background material signatures act as a secondary source of noise when considering the concatenated set of patches. Thus, for sufficiently high SNR the effect of the varying background on performance is more significant than the effect of additive noise, leading to a lower bound for SAD. Our proposed algorithms account for varying background material signatures among patches, so we do not observe the same issue in these methods. This explanation is further supported by the effect of changing the ratio of expected magnitudes of background material signature components. As we increase the ratio (from subfigures (a) to (c) and from subfigures (d) to (f)), the background material signatures become more varied between patches. Subsequently, the minimum SAD observed for the benchmark algorithm increases. Again, our proposed algorithms are designed to allow for varying background material signatures, so we do not see a notable impact on the performance of these methods.

The poor performance of BMMF-LS-NM is expected in this setting, as the data does not satisfy the necessary conditions of the algorithm. First, given  $r$  spectral signatures in the data, the number of spectral bands required in each signature is of order  $O(r^4)$ . In this setting, there are 11 spectral signatures corresponding to 10 distinct background materials and one foreground material, while there are only 30 spectral bands for each signature. Additionally, the (noiseless) set of pixels needs to have rank equal to the number of spectral signatures and bilinear combinations. With 11 spectral signatures, the necessary rank is 55. However, each patch is a rank 2 span between the background-illumination signature for the patch and its product with the foreground material signature. With 10 patches, the rank of the noiseless data is at most 20. Thus, the theoretical guarantees for performance of BMMF-LS-NM are not met. The poor performance of SNPALQ is also expected in this setting, as the algorithm extracts spectral signatures by identifying pure pixels in the data. As the foreground material never appears in isolation from background materials, there is no pure pixel corresponding to the foreground material signature, and all the estimated material signatures will be distinct from the true foreground material signature.

In comparing the performance of our proposed methods, we observe that for a given value of SNR, the MinVolFit algorithm achieves a smaller mean SAD than the EPFit algorithm for at least one choice of hyperparameter. This is reasonable: the EPFit algorithm produces an estimate of the foreground material signature by identifying two endpoints in a set of patches and computing their elementwise ratio. Any noise affecting these endpoints will directly affect this ratio, and therefore the

estimate of the foreground material signature. In contrast, the MinVolFit algorithm can accommodate some amount of noise via careful selection of the regularization weight  $\tau$ . Any non-zero value of  $\tau$  allows a slight increase in fitting error if it allows a decrease in the volume measure, which can allow the estimated foreground material signature to have a smaller volume measure than would be given by noisy endpoints. However, selecting an optimal regularization weight is non-trivial. In contrast, the EPFit algorithm does not require any hyperparameter selection.

## B. Real Data Experiments

To verify that our algorithms can perform in a practical setting with potentially unknown variations, we consider experiments in a real data scenario. Our goals for real data experiments are as follows: to demonstrate that algorithms which account for per-patch background variation can perform better than algorithms which do not take such variation into account; and to verify that our algorithms have some robustness to unknown variations that may be present in real data. We will show that our algorithms, which can adapt to varying backgrounds per patch, will obtain more accurate foreground material signature estimates than a benchmark algorithm which does not account for varying backgrounds. For the MinVolFit algorithm, we will show that for an appropriate choice of regularization weight the estimated foreground material signature will be close to the expected signature. Similarly, for the EPFit algorithm we will show that the estimated foreground material signature will be close to the expected signature.

**Data sampling:** We use the dataset created by Kendler et al. [9]. The dataset consists of several annotated hyperspectral cubes of a particular scene. The scene consists of many background materials, with a mix of five distinct foreground materials (sugar, polystyrene, silicone, white silicone, and jam) deposited on the surfaces of several background materials. A depiction of this dataset is provided in Figure 2 of [9]. The locations of background and foreground materials in the scene are annotated in the dataset. However, the specific coverage at the per-pixel level is unknown; the annotation specifies only whether a pixel contains any amount foreground material. To facilitate experiments, we selected regions containing two different background materials (ceramic tile and plywood) and one shared foreground material (silicone deposit). We sampled patches by sweeping a  $12 \times 12$  square window with a one-pixel offset through each region.

**Algorithms:** To account for the significant noise present in real data, we make a slight modification to the EPFit algorithm. In this, the matrix  $\tilde{Y}$  contains the vectors of all patches projected onto a rank-2 span. The final step of the algorithm is to find the pair of vectors with maximum SAD, under the assumption that these vectors represent endpoints in the original data. In the presence of noise, it is possible for vectors which are not endpoints to be perturbed such that they produce a larger SAD with respect to other vectors in the span than the true endpoints. To account for these possible errors, we consider removing



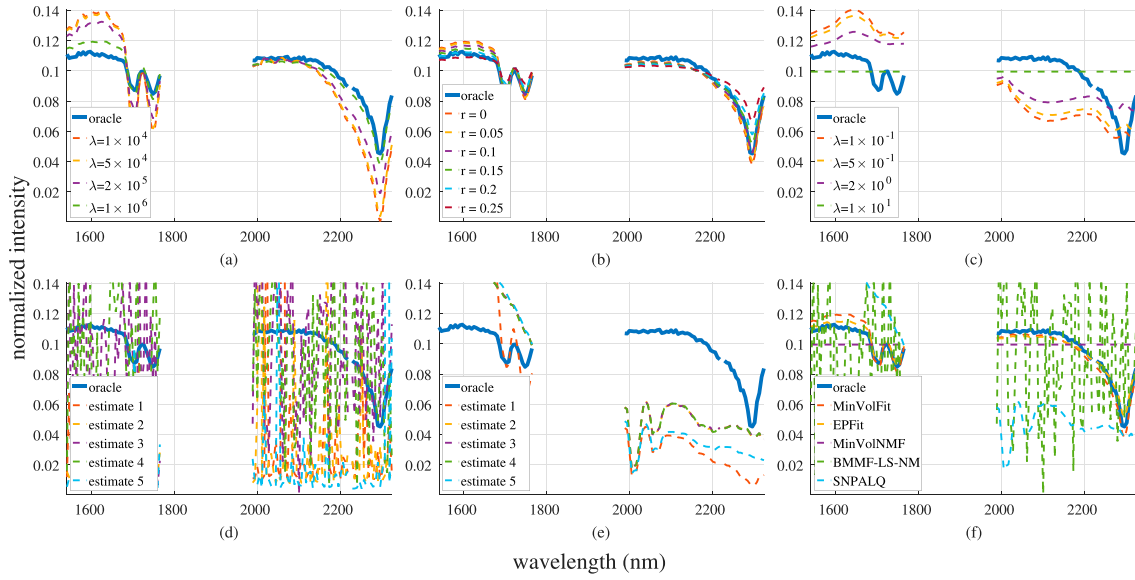


Fig. 3. Recovered foreground material signatures of a silicone deposit on both ceramic tile and plywood backgrounds obtained using (a) the proposed MinVolFit algorithm with various choices of regularization weight  $\lambda$ ; (b) the proposed EPFit algorithm with various choices of endpoint removal ratio  $r$ ; (c) the MinVolNMF benchmark algorithm with various choices of regularization weight  $\lambda$ ; (d) the five best estimates produced by the BMMF-LS-NM benchmark algorithm; (e) the five best estimates produced by the SNPALQ algorithm. The figure (f) shows a collection of the most accurate estimated foreground material signatures (by smallest SAD from oracle signature) obtained with each method.

some proportion  $r$  of columns from  $\tilde{Y}$  which yield the largest SAD. In addition, we change the hyperparameters of SNPALQ to account for the unknown number of true spectral signatures in the data. From our modeling assumptions, we infer an upper bound on the number of spectral signatures as the sum of the number of patches (one background signature per patch) plus the foreground material signature. From our sampling approach, we infer a lower bound as the sum of the two background materials (at least signature each) and the foreground material signature. We provide these bounds for hyperparameters in SNPALQ.

**Evaluation scheme:** Unlike the synthetic data experiments, the true foreground material signatures for the real data experiments are unknown. However, with the label information for the locations of foreground and background materials, we can make a reasonable inference as to the value of the true foreground material signature up to scaling and noise effects. Given a region containing exactly one background and foreground material, we may compare all possible foreground pixels with all possible background pixels and extract candidate foreground signatures by taking the elementwise ratio of these combinations. To avoid issues of small variations in the background material, we select pairs of pixels that are within 10 pixels of each other. This is similar to the background subtraction method in [9]. Then, we may sort all candidate foreground material signatures by their volume measure (see (8)) and obtain a denoised reference foreground material signature by averaging the top  $k$  signatures. For our experiments, we let  $k = 10$ .

**Results and Analysis:** Results for foreground signature extraction of silicone deposit on ceramic tile and plywood are shown in Fig. 3. We observe that for all three of our algorithms, there is a choice of hyperparameter that yields a foreground signature

TABLE I  
TOTAL RUNTIME AND AVERAGE PER-ITERATION RUNTIME FOR  
VARIOUS ALGORITHMS AND BENCHMARKS

Algorithm	$\lambda, r, \mu$	Total Time (s)	Avg. Per-Iter. Time (s)
MinVolFit	$10^4$	$2.217 \times 10^2$	$2.508 \times 10^{-1}$
	$5 \times 10^4$	$2.479 \times 10^2$	
	$2 \times 10^5$	$3.111 \times 10^2$	
	$10^6$	$2.239 \times 10^2$	
EPFit	all	$2.454 \times 10^2$	$2.454 \times 10^{-1}$
MinVolNMF	0.1	$3.162 \times 10^1$	$3.172 \times 10^{-2}$
	0.5	$3.097 \times 10^1$	
	2	$3.264 \times 10^1$	
	10	$3.168 \times 10^1$	

estimate that is close to the reference signature. In contrast, all three benchmarks show some difference between the estimates and reference. In particular, the MinVolNMF and BMMF-LS-NM algorithms show significant deviation from the reference signature. For MinVolNMF, this is expected as the approach is to concatenate all patches and solve for endpoint vectors as a rank-2 NMF problem, an assumption which does not hold when we consider a scenario with multiple backgrounds. For BMMF-LS-NM, the theoretical guarantees for the algorithm are not met in a similar manner to the synthetic data experiments.

## VI. CONCLUSION

In this paper, we explored the problem of foreground material signature extraction under an intimate mixing bag-of-patches model. The problem of non-uniqueness of the solution for the foreground signature was identified and the space of all feasible solutions was derived. Conditions and criteria under

which identifiable solutions are guaranteed were suggested and proven. Several algorithms with identifiability guarantees were proposed based on the previously suggested criteria. Experiments on synthetic data demonstrated the capability of the proposed algorithms to obtain identifiable solutions in settings where existing methods do not succeed.

This paper considers the specific case of one foreground material deposited on several background materials. A more general model may consider the case of multiple foreground materials. Foreground materials may still appear isolated per pixel, or may appear in combination within individual pixels. A further extension of the model would be to remove the restriction of each patch containing only one background material. This would remove the need to carefully select patches. Our current theory on identifiability in the bag-of-patches model is not sufficient to handle these extended models, but may serve as a good foundation for analysis of an extended model.

## APPENDIX

### A. Proof of Theorem 1

We use the following result in the proof of Theorem 1:

**Lemma 3:** Assume  $\mathbf{s} = c(t\mathbf{v} + (1-t)\mathbf{1}) \odot (u\mathbf{v} + (1-u)\mathbf{1})$  with  $c > 0$  and  $\mathbf{v}$  strictly positive such that  $\mathbf{v} \odot \mathbf{v}, \mathbf{v}, \mathbf{1}$  are independent. Let  $K_1(\mathbf{s}) = \|\mathbf{s}\|^2 \|\mathbf{1}\|^2 - (\mathbf{s}^T \mathbf{1})^2$  and  $K_2(\mathbf{s}) = -(\|\mathbf{s}\|^4 - (\mathbf{s}^T (\mathbf{s} \odot \mathbf{s}))(\mathbf{s}^T \mathbf{1}))$ . If  $t - u \neq 0$ , then

- 1)  $\mathbf{1}, \mathbf{s}$ , and  $\mathbf{s} \odot \mathbf{s}$  are linearly independent and
- 2)  $K_1(\mathbf{s})$  and  $K_2(\mathbf{s})$  are strictly positive.

The proof of Lemma 3 is given in the supplementary material. We proceed with the proof of Theorem 1:

**Proof:** Let  $\mathcal{S}$  be the set of all feasible solutions as given in Proposition 1. For every feasible solution  $\mathbf{s} \in \mathcal{S}$ , there must exist parameters  $\alpha, \beta, \gamma, \delta$  such that the following hold:

$$\begin{aligned} \mathbf{s} &= (\alpha \mathbf{f} + \beta \mathbf{1}) \odot (\gamma \mathbf{f} + \delta \mathbf{1}), \\ \frac{\delta - \gamma r_a}{\alpha \delta - \beta \gamma} &\geq 0, \quad \frac{\delta r_b - \gamma}{\alpha \delta - \beta \gamma} \geq 0, \quad \frac{\alpha - \beta r_b}{\alpha \delta - \beta \gamma} \geq 0, \quad \frac{\alpha r_a - \beta}{\alpha \delta - \beta \gamma} \geq 0, \\ \alpha \max f_i + \beta &> 0, \quad \alpha \min f_i + \beta > 0, \\ \gamma \max f_i + \delta &> 0, \quad \gamma \min f_i + \delta > 0, \\ \text{and } \alpha \delta - \beta \gamma &\neq 0, \end{aligned} \quad (19)$$

where  $r_a$  and  $r_b$  are defined as in (7). The volume-minimization problem in Definition 2, i.e., the volume minimization of (8) may be replaced with the following maximization problem:

$$\max_{\mathbf{s} \in \mathcal{S}} g(\mathbf{s}) = \frac{(\mathbf{s}^T \mathbf{1})}{\|\mathbf{s}\|_2}. \quad (20)$$

**Reparameterization:** Before we proceed, we would like to point out that w.l.o.g. we make the assumption that  $\min_i f_i < 1 < \max_i f_i$ .<sup>5</sup> Consider the following reparameterization of the problem using

$$\mathbf{s} = c(t\mathbf{f} + (1-t)\mathbf{1}) \odot (u\mathbf{f} + (1-u)\mathbf{1}). \quad (21)$$

<sup>5</sup>Note that since  $\mathbf{f}$  is linearly independent of  $\mathbf{1}$ , it cannot be constant and hence  $\min_i f_i < \max_i f_i$ . To ensure that  $\mathbf{f}$  used in the proof satisfies  $\min_i f_i < 1 < \max_i f_i$ , a scaling can be applied to the original  $\mathbf{f}$  so that  $\mathbf{s}$  is defined in terms of the scaled version of  $\mathbf{f}$  without loss of generality.

Every element in  $\mathcal{S}$  has a representation in  $(c, t, u)$ . To show this, note that every element  $\mathbf{s} \in \mathcal{S}$  can be parameterized by  $(\alpha, \beta, \gamma, \delta)$ . Consider

$$\begin{aligned} \mathbf{s} &= (\alpha \mathbf{f} + \beta \mathbf{1}) \odot (\gamma \mathbf{f} + \delta \mathbf{1}) \\ &= \frac{\gamma + \delta}{\alpha + \beta} \left( \frac{\alpha}{\alpha + \beta} \mathbf{f} + \frac{\beta}{\alpha + \beta} \mathbf{1} \right) \odot \left( \frac{\gamma}{\gamma + \delta} \mathbf{f} + \frac{\delta}{\gamma + \delta} \mathbf{1} \right). \end{aligned} \quad (22)$$

Note that dividing by  $\alpha + \beta$  and  $\gamma + \delta$  is always well-defined. Suppose  $\alpha + \beta = 0$ : then  $\alpha \min f_i + \beta = \alpha(\min f_i - 1) \leq 0$  (by assumption that  $\min f_i < 1$ ). This violates the constraint in (19), so  $\alpha + \beta$  must be non-zero. This follows similarly for  $\gamma + \delta$ . Finally, taking  $c = (\gamma + \delta)(\alpha + \beta)$ ,  $t = \alpha/(\alpha + \beta)$ , and  $u = \beta/(\alpha + \beta)$ , we have that  $\mathbf{s}$  has a representation in  $(c, t, u)$ .

The mapping  $(c, t, u) \mapsto \mathbf{s}$  is bijective for feasible solutions (see proof in supplementary material). Further, the manifold produced by this mapping is differentiable everywhere. To show this, consider the Jacobian of  $\mathbf{s}$  with respect to the parameter vector  $\theta = [c, t, u]^T$ :

$$\frac{d\mathbf{s}}{d\theta^T} = \frac{1}{c(t-u)} \begin{bmatrix} \mathbf{s} \odot \mathbf{s} & \mathbf{s} & \mathbf{1} \end{bmatrix} \begin{bmatrix} 0 & 0 & -1 \\ t-u & cc & 0 \\ 0 & -c^2 & 0 \end{bmatrix}. \quad (23)$$

The Jacobian is well-defined within the set of feasible solutions.<sup>6</sup> The determinant of the matrix on the right is  $\det = c^2(t-u)$ , which is strictly non-zero for all feasible  $\mathbf{s}$  as  $c > 0$  and  $t-u \neq 0$ , and therefore this matrix has full rank. The columns  $\mathbf{s} \odot \mathbf{s}, \mathbf{s}$ , and  $\mathbf{1}$  in the matrix on the left are linearly independent, so this matrix also has full rank. Then the Jacobian has full rank in the set of feasible solutions. Thus, the mapping  $(c, t, u) \mapsto \mathbf{s}$  is differentiable everywhere within the feasibility set of the maximization problem. In summary, the mapping  $(c, t, u) \mapsto \mathbf{s}$  produces a differentiable manifold, and therefore we may recast the problem of maximization over  $\mathbf{s}$  into a problem of maximization over  $(c, t, u)$ .

Using the new parameterization, the volume minimization problem can be recast as follows

$$\begin{aligned} \max_{c, t, u} \quad & g(\mathbf{s}) = \frac{(\mathbf{s}^T \mathbf{1})}{\|\mathbf{s}\|_2} \\ \text{s.t.} \quad & \frac{1-u-ur_a}{c(t-u)} \geq 0, \quad \frac{(1-u)r_b-u}{c(t-u)} \geq 0, \\ & \frac{c(t-(1-t)r_b)}{c(t-u)} \geq 0, \quad \frac{c(tr_a-(1-t))}{c(t-u)} \geq 0, \\ & c(t \max f_i + (1-t)) > 0, \quad c(t \min f_i + (1-t)) > 0, \\ & u \max f_i + (1-u) > 0, \quad u \min f_i + (1-u) > 0, \\ & \text{and } c(t-u) \neq 0. \end{aligned} \quad (24)$$

**Finding local maxima:** Let  $\theta = [c, t, u]^T$ . To identify local maxima, we can consider the maximization over  $c(t-u) > 0$  and over  $c(t-u) < 0$  as two separate maximization problems

<sup>6</sup>Simple algebraic manipulation of the Jacobian shows that the denominator  $c(t-u)$  cancels out of each term in the Jacobian. The Jacobian is undefined only if  $uf_i + (1-u) = 0$  for some  $i$ , which violates the feasibility constraints.

and identify local maxima in each. First, assume  $c(t - u) > 0$ . If  $c(t - u) > 0$ , then we can rewrite the problem as

$$\begin{aligned} \max_{\theta} \quad & g(\mathbf{s}) = \frac{(\mathbf{s}^T \mathbf{1})}{\|\mathbf{s}\|_2} \\ \text{s.t.} \quad & 1 - u - ur_a \geq 0, \quad (1 - u)r_b - u \geq 0, \\ & c(t - (1 - t)r_b) \geq 0, \quad c(tr_a - (1 - t)) \geq 0, \\ & c(t \max f_i + (1 - t)) > 0, \quad c(t \min f_i + (1 - t)) > 0, \\ & u \max f_i + (1 - u) > 0, \quad u \min f_i + (1 - u) > 0, \\ & c(t - u) > 0. \end{aligned} \quad (25)$$

The constraints simplify to  $t \in [(1 + r_a)^{-1}, (1 - \min f_i)^{-1}]$ ,  $u \in [-(\max f_i - 1)^{-1}, r_b/(1 + r_b)]$ , and  $c > 0$ . The derivation of this simplified set of constraints is given in the supplementary material. Note that  $r_b/(1 + r_b) < 1/(1 + r_a)$ , so  $t > u$  and hence  $c(t - u) > 0$  holds implicitly. Denote the feasibility set containing all  $\theta$  which satisfy the aforementioned constraints by  $\Theta_1$ . We can write the maximization as

$$\max_{\theta \in \Theta_1} J(c, t, u), \quad (26)$$

where  $J(c, t, u) = \mathbf{s}^T(c, t, u)\mathbf{1}/\|\mathbf{s}(c, t, u)\|$ .<sup>7</sup> To show the existence of a local maximum, we consider the derivative of the objective with respect to  $\theta$ :

$$\begin{aligned} dJ/d\theta^T &= \frac{1}{(t - u)\|\mathbf{s}\|^3} [0, -cK_1(\mathbf{s}), \frac{1}{c}K_2(\mathbf{s})], \\ K_1(\mathbf{s}) &= \|\mathbf{s}\|^2 \|\mathbf{1}\|^2 - (\mathbf{s}^T \mathbf{1})^2, \\ K_2(\mathbf{s}) &= (\mathbf{s}^T (\mathbf{s} \odot \mathbf{s}))(\mathbf{s}^T \mathbf{1}) - \|\mathbf{s}\|^4. \end{aligned} \quad (27)$$

The computation of this derivative is given in the supplementary material. Note that  $c > 0$  and  $c(t - u) > 0$  for any  $\theta \in \Theta_1$ , and therefore  $t - u > 0$ . Given that  $t - u \neq 0$ , it follows from Lemma 3 that  $K_1(\mathbf{s})$  and  $K_2(\mathbf{s})$  are both strictly positive. Based on the derivative, the objective is constant along  $c$ , monotonically decreasing along  $t$ , and monotonically increasing along  $u$ . Our feasibility set is defined by box constraints on  $t$  and  $u$ , so a local maximum is obtained for any  $c^* > 0$  at the lower bound for  $t$  and the upper bound for  $u$ . At any other point, it is possible to either move in decreasing  $t$  or increasing  $u$  and further increase the objective. Thus, a local maximum only exists at  $(c, (1 + r_a)^{-1}, r_b/(1 + r_b))$  for any  $c > 0$ . Substituting the parameters for a local maximum yields

$$\mathbf{s} = \frac{c(1 + r_b)}{1 + r_a} (\mathbf{f} + r_a \mathbf{1}) \odot (r_b \mathbf{f} + \mathbf{1}) = c' \mathbf{f}_0. \quad (28)$$

Due to space limitations, we omit the derivation for the negative sign case, which can be derived using a similar approach as to the positive sign case. In the case of negative sign, it holds that  $\mathbf{s} = c' \mathbf{f}_0^{-1}$ .  $\square$

## B. Proof of Theorem 2

*Proof:* Let  $\mathcal{Y} = \{\mathbf{Y}^{(1)}, \dots, \mathbf{Y}^{(K)}\}$  be a set of patches following the bag-of-patches model in (5) with a true foreground material signature  $\mathbf{f} \in \mathbb{R}_{++}^M$ , and assume  $\mathbf{1}, \mathbf{f}, \mathbf{f} \odot \mathbf{f}$  are

linearly independent. We will begin by showing that any endpoint fit solution  $\mathbf{f}^*$  satisfies  $\mathbf{f}^* = c\mathbf{f}_0$  or  $\mathbf{f}^* = c\mathbf{1} \odot \mathbf{f}_0$ .

**Forward direction:** Let  $\mathbf{f}^*$  be an endpoint fit solution. As  $\mathbf{1}, \mathbf{f}, \mathbf{f} \odot \mathbf{f}$  are linearly independent, Property 1 is applicable. According to Property 1, every coefficient matrix of a feasible solution has the form

$$\tilde{\mathbf{C}}^{(k)} = \frac{1}{\epsilon_k} \begin{bmatrix} \alpha & \gamma \\ \beta & \delta \end{bmatrix}^{-1} \mathbf{C}^{(k)} \quad (29)$$

where  $\epsilon_k > 0$  and  $\alpha\delta - \beta\gamma \neq 0$ . The  $i$ th column of the  $k$ th coefficient matrix is therefore

$$\tilde{\mathbf{c}}_i^{(k)} = \frac{1}{\epsilon_k(\alpha\delta - \beta\gamma)} \begin{bmatrix} \delta c_{1i}^{(k)} - \gamma c_{2i}^{(k)} \\ \alpha c_{2i}^{(k)} - \beta c_{1i}^{(k)} \end{bmatrix}. \quad (30)$$

Note that the coefficient matrices  $\tilde{\mathbf{C}}^{(k)}$  for  $k = 1, \dots, K$  must be non-negative (see Definition 1). Recall also that  $\epsilon_k > 0$ . Then for all  $i$  and  $k$ , the following inequalities must hold:

$$\frac{\delta c_{1i}^{(k)} - \gamma c_{2i}^{(k)}}{\alpha\delta - \beta\gamma} \geq 0 \quad \text{and} \quad \frac{\alpha c_{2i}^{(k)} - \beta c_{1i}^{(k)}}{\alpha\delta - \beta\gamma} \geq 0. \quad (31)$$

Recall the definition of an endpoint fit solution: there exists indices  $k_1$  and  $k_2$  such that  $\tilde{\mathbf{C}}^{(k_1)}$  contains a column  $[x, 0]^T$  and  $\tilde{\mathbf{C}}^{(k_2)}$  contains a column  $[0, y]^T$  where  $x, y > 0$ . Thus, an endpoint fit solution must satisfy the inequalities in (31) for every column of every coefficient matrix, and must satisfy the two equality conditions for some column(s). The set of endpoint fit solutions is therefore all choices of  $\alpha, \beta, \gamma, \delta$  such that the following hold:

$$\begin{aligned} \frac{\delta c_{1i}^{(k)} - \gamma c_{2i}^{(k)}}{\alpha\delta - \beta\gamma} &\geq 0 \quad \text{and} \quad \frac{\alpha c_{2i}^{(k)} - \beta c_{1i}^{(k)}}{\alpha\delta - \beta\gamma} \geq 0, \quad \forall i, k, \\ \exists i_1, k_1 \quad \text{s.t.} \quad &\delta c_{1i_1}^{(k_1)} - \gamma c_{2i_1}^{(k_1)} = 0, \\ \exists i_2, k_2 \quad \text{s.t.} \quad &\alpha c_{2i_2}^{(k_2)} - \beta c_{1i_2}^{(k_2)} = 0. \end{aligned} \quad (32)$$

We consider two cases based on the sign of  $\alpha\delta - \beta\gamma$ . First, assume  $\alpha\delta - \beta\gamma > 0$ . The set defined by (32) simplifies to

$$\begin{aligned} \alpha c_{2i}^{(k)} - \beta c_{1i}^{(k)} &\geq 0 \quad \text{and} \quad \delta c_{1i}^{(k)} - \gamma c_{2i}^{(k)} \geq 0, \quad \forall i, k, \\ \exists i_1, k_1 \quad \text{s.t.} \quad &\alpha c_{2i_1}^{(k_1)} - \beta c_{1i_1}^{(k_1)} = 0, \\ \exists i_2, k_2 \quad \text{s.t.} \quad &\delta c_{1i_2}^{(k_2)} - \gamma c_{2i_2}^{(k_2)} = 0. \end{aligned} \quad (33)$$

Let  $\mathcal{S}_1 = \{(i, k) \mid c_{1i}^{(k)} \neq 0\}$ , and let  $\mathcal{S}'_1 = \{(i, k) \mid c_{1i}^{(k)} = 0\}$ . The sets  $\mathcal{S}_1$  and  $\mathcal{S}'_1$  partition the set of all indices. The requirement that each  $\mathbf{Y}^{(k)}$  is rank 2 implies that each  $\mathbf{C}^{(k)}$  is rank 2, and therefore  $\mathcal{S}_1$  is non-empty.<sup>8</sup> Further, the restriction that no column of  $\mathcal{Y}^{(k)}$  for all  $k$  is a zero-valued column implies that  $c_{1i}^{(k)} \neq 0$  for all  $(i, k) \in \mathcal{S}'_1$ . Consider the constraints on  $\alpha$  and  $\beta$ , partitioned by  $\mathcal{S}_1$  and  $\mathcal{S}'_1$ :

$$\begin{aligned} \beta &\leq \alpha \frac{c_{2i}^{(k)}}{c_{1i}^{(k)}}, \quad \forall (i, k) \in \mathcal{S}_1, \\ 0 &\leq \alpha, \quad \forall (i, k) \in \mathcal{S}'_1, \\ \exists (i_1, k_1) \in \mathcal{S}_1 \quad \text{s.t.} \quad &\beta = \alpha \frac{c_{2i_2}^{(k_2)}}{c_{1i_2}^{(k_2)}} \quad \text{or} \quad \exists (i_1, k_1) \in \mathcal{S}'_1 \quad \text{s.t.} \quad \alpha = 0. \end{aligned} \quad (34)$$

<sup>8</sup>If  $\mathcal{S}_1$  is empty, then  $c_{1i}^{(k)} = 0$  and therefore every  $\mathbf{C}^{(k)}$  is rank 1, which is a contradiction.



We may discard the case of  $\exists(i_1, k_1) \in \mathcal{S}'_1$  s.t.  $\alpha = 0$ , as this implies  $\beta \leq 0$  and therefore  $\alpha\mathbf{f} + \beta\mathbf{1} \leq 0$ , which contradicts P1:2 in Proposition 1. Then we are left with the case of  $\exists(i_1, k_1) \in \mathcal{S}_1$  s.t.  $\beta = \alpha c_{2i_2}^{(k_2)} / c_{1i_2}^{(k_2)}$ . For  $\beta$  to be both a lower bound of the set  $\{\alpha c_{2i}^{(k)} / c_{1i}^{(k)}\}_{\forall(i,k) \in \mathcal{S}_1}$  and equal to an element of the set, it must hold that  $\beta = \min_{i,k} \alpha c_{2i}^{(k)} / c_{1i}^{(k)}$ , where  $c_{2i}^{(k)} / c_{1i}^{(k)}$  is defined as  $\infty$  if  $c_{1i}^{(k)} = 0$ . Note that if  $\alpha = 0$ , then  $\beta = 0$  and therefore  $\alpha\delta - \beta\gamma = 0$ , which is a contradiction. Also, if  $\alpha < 0$  then  $\beta \leq 0$ , and therefore  $\alpha\mathbf{f} + \beta\mathbf{1} < 0$ , which contradicts P1:2 in Proposition 1. Then it must hold that  $\alpha > 0$ , and therefore an endpoint satisfies  $\alpha = \beta \min_{i,k} c_{2i}^{(k)} / c_{1i}^{(k)} = \delta r_a$  (see (7)).

Now, we will consider the constraints on  $\gamma$  and  $\delta$ . Let  $\mathcal{S}_2 = \{(i, k) \mid c_{2i}^{(k)} \neq 0\}$ , and let  $\mathcal{S}'_2 = \{(i, k) \mid c_{2i}^{(k)} = 0\}$ . The sets  $\mathcal{S}_2$  and  $\mathcal{S}'_2$  partition the set of all indices. Note that  $\mathcal{S}_2$  is non-empty, and  $c_{2i}^{(k)} \neq 0$  for all  $(i, k) \in \mathcal{S}'_2$ , by similar reasoning as above. The constraints on  $\gamma$  and  $\delta$ , partitioned by  $\mathcal{S}_1$  and  $\mathcal{S}'_1$ , may be expressed as

$$\begin{aligned} \gamma &\leq \delta \frac{c_{1i}^{(k)}}{c_{2i}^{(k)}}, \quad \forall(i, k) \in \mathcal{S}_2, \quad 0 \leq \delta, \quad \forall(i, k) \in \mathcal{S}'_2, \\ \exists(i_2, k_2) \in \mathcal{S}_2 \text{ s.t. } \gamma &= \delta \frac{c_{1i_2}^{(k_2)}}{c_{2i_2}^{(k_2)}} \quad \text{or} \quad \exists(i_2, k_2) \in \mathcal{S}'_2 \text{ s.t. } \delta = 0. \end{aligned} \quad (35)$$

We may discard the case of  $\exists(i_2, k_2) \in \mathcal{S}'_2$  s.t.  $\delta = 0$ , as this implies  $\gamma \leq 0$  and therefore  $\gamma\mathbf{f} + \delta\mathbf{1} \leq 0$ , which contradicts P1:3 in Proposition 1. Then we are left with the case of  $\exists(i_2, k_2) \in \mathcal{S}_2$  s.t.  $\gamma = \delta c_{1i_2}^{(k_2)} / c_{2i_2}^{(k_2)}$ . For  $\gamma$  to be both a lower bound of the set  $\{\delta c_{1i}^{(k)} / c_{2i}^{(k)}\}_{\forall(i,k) \in \mathcal{S}_2}$  and equal to an element of the set, it must hold that  $\gamma = \min_{i,k} \delta c_{1i}^{(k)} / c_{2i}^{(k)}$ , where  $c_{1i}^{(k)} / c_{2i}^{(k)}$  is defined as  $\infty$  if  $c_{2i}^{(k)} = 0$ . Note that if  $\delta = 0$ , then  $\gamma = 0$  and therefore  $\alpha\delta - \beta\gamma = 0$ , which is a contradiction. Also, if  $\delta < 0$  then  $\gamma \leq 0$ , and therefore  $\gamma\mathbf{f} + \delta\mathbf{1} < 0$ , which contradicts P1:3 in Proposition 1. Then it must hold that  $\delta > 0$ . Therefore, an endpoint satisfies  $\gamma = \delta \min_{i,k} c_{1i}^{(k)} / c_{2i}^{(k)} = \delta r_b$  (see (7)).

Note that for  $\beta = \alpha r_a$  and  $\gamma = \delta r_b$ , it holds that  $\alpha\delta - \beta\gamma = \alpha\delta(1 - r_a r_b) > 0$ . Finally, we have

$$\begin{aligned} \mathbf{f}^* &= (\alpha\mathbf{f} + \beta\mathbf{1}) \odot (\beta\mathbf{f} + \gamma\mathbf{1}) \\ &= \frac{\alpha}{\delta} (\mathbf{f} + r_a\mathbf{1}) \odot (r_b\mathbf{f} + \mathbf{1}) = c\mathbf{f}_0. \end{aligned} \quad (36)$$

Due to space limitations, we omit the derivation for the negative sign case, which can be derived using a similar approach as to the positive sign case. In the case of negative sign, it holds that  $\mathbf{f}^* = c\mathbf{1} \odot \mathbf{f}_0$ .

**Backward direction:** Let  $\mathbf{f}^* = c\mathbf{f}_0 = (c\mathbf{f} + cr_a\mathbf{1}) \odot (r_b\mathbf{f} + \mathbf{1})$ . We will use Property 1 to show that such a solution is an endpoint fit solution. A matching parameterization is  $(\alpha, \beta, \gamma, \delta) = (c, cr_a, r_b, 1)$ . From Property 1, the  $i$ th column of the  $k$ th coefficient matrix is

$$\bar{\mathbf{c}}_i^{(k)} = \frac{1}{\epsilon_k c(1 - r_a r_b)} \begin{bmatrix} c_{1i}^{(k)} - r_b c_{2i}^{(k)} \\ c c_{2i}^{(k)} - c r_a c_{1i}^{(k)} \end{bmatrix}, \quad (37)$$

where  $\epsilon_k > 0$ . Recall that  $r_a := \min_{i,k} c_{2i}^{(k)} / c_{1i}^{(k)}$  and  $r_b := \min_{i,k} c_{1i}^{(k)} / c_{2i}^{(k)}$ . Let  $(i_1, k_1) = \arg \min_{i,k} c_{2i}^{(k)} / c_{1i}^{(k)}$ . Then

$$c c_{2i_1}^{(k_1)} - c r_a c_{1i_1}^{(k_1)} = c(c_{2i_1}^{(k_1)} - \frac{c_{2i_1}^{(k_1)}}{c_{1i_1}^{(k_1)}} c_{1i_1}^{(k_1)}) = 0. \quad (38)$$

Letting  $(i_2, k_2) = \arg \min_{i,k} c_{1i}^{(k)} / c_{2i}^{(k)}$ , it holds that

$$c_{1i_2}^{(k_2)} - r_b c_{2i_2}^{(k_2)} = c_{1i_2}^{(k_2)} - \frac{c_{1i_2}^{(k_2)}}{c_{2i_2}^{(k_2)}} c_{2i_2}^{(k_2)} = 0. \quad (39)$$

Thus, for solutions of the form  $\mathbf{f}^* = c\mathbf{f}_0$ , the conditions for an endpoint fit solution are satisfied. The argument for solutions of the form  $\mathbf{f}^* = c\mathbf{1} \odot \mathbf{f}_0$  follows similarly.  $\square$

### C. Proof of Lemma 1

*Proof:* Let  $\mathbf{C}^{(k)} \in \mathbb{R}_+^{2 \times N_k}$  for  $k = 1, 2, \dots, K$  be elementwise non-negative matrices where no column is equal to the zero vector and at least one matrix is full row-rank. Let  $\mathbf{C} = [\mathbf{C}^{(1)} \dots \mathbf{C}^{(K)}]$ . Note that  $\mathbf{C}$  must also be full row-rank due to at least one of  $\mathbf{C}^{(1)}, \dots, \mathbf{C}^{(K)}$  having full row-rank. For any invertible matrix  $\mathbf{T} \in \mathbb{R}^{2 \times 2}$ , we have  $\mathbf{T}^{-1}\mathbf{C} = \mathbf{T}^{-1}[\mathbf{C}^{(1)} \dots \mathbf{C}^{(K)}] = [\mathbf{T}^{-1}\mathbf{C}^{(1)} \dots \mathbf{T}^{-1}\mathbf{C}^{(K)}]$ . Hence, if the matrix on the left  $\mathbf{T}^{-1}\mathbf{C}$  is elementwise non-negative the matrix on the right is elementwise non-negative or equivalently its submatrices  $\mathbf{T}^{-1}\mathbf{C}^{(k)}$  for  $k = 1, 2, \dots, K$  are elementwise non-negative. Similarly, if we define the  $i$ th column of  $\mathbf{C}$  as  $\mathbf{c}_i$ , then  $\mathbf{C} = [\mathbf{c}_1 \dots \mathbf{c}_n]$  and consequently  $\mathbf{T}^{-1}\mathbf{C} = [\mathbf{T}^{-1}\mathbf{c}_1 \dots \mathbf{T}^{-1}\mathbf{c}_n]$ . Elementwise non-negativity of the LHS implies the elementwise non-negativity of the RHS and vice versa, i.e.,  $\mathbf{T}^{-1}\mathbf{C} \geq 0$  if and only if  $\mathbf{T}^{-1}\mathbf{c}_i \geq 0, \forall i$ . Thus,

$$\mathbf{T}^{-1}\mathbf{C}^{(k)} \geq 0, \forall k \iff \mathbf{T}^{-1}\mathbf{c}_i \geq 0, \forall i. \quad (40)$$

Consider the inequality on the RHS of (40). Since multiplication by a non-negative constant preserves the inequality, we have  $\mathbf{T}^{-1}\mathbf{c}_i \geq 0 \iff \gamma_i \mathbf{T}^{-1}\mathbf{c}_i \geq 0 \iff \mathbf{T}^{-1}\gamma_i \mathbf{c}_i \geq 0$  for all  $i$ , where  $\gamma_i > 0$ . Using that no column is equal to the zero vector, we can define a scaling term  $\gamma_i = 1/(c_{1i} + c_{2i})$  for the  $i$ th column for all  $i$ . Using this choice of  $\gamma_i$ , we can introduce the scaled  $i$  column  $\bar{\mathbf{c}}_i = \gamma_i \mathbf{c}_i = [\frac{c_{1i}}{c_{1i} + c_{2i}}, \frac{c_{2i}}{c_{1i} + c_{2i}}]^T$ . Therefore, we have

$$\mathbf{T}^{-1}\mathbf{c}_i \geq 0, \forall i \iff \mathbf{T}^{-1}\bar{\mathbf{c}}_i \geq 0, \forall i. \quad (41)$$

Define  $\alpha_i = c_{1i}/(c_{1i} + c_{2i})$ ; the scaled  $i$ th column may be expressed as  $\bar{\mathbf{c}}_i = [\alpha_i, 1 - \alpha_i]^T$ . Let  $a = \arg \max_i \alpha_i$  and  $b = \arg \min_i \alpha_i$ . Let  $\bar{\alpha}_i = \frac{\alpha_i - \alpha_b}{\alpha_a - \alpha_b}$ . Since every  $\alpha_i \in [\alpha_a, \alpha_b]$ , it holds that  $\bar{\alpha}_i \in [0, 1]$ . Using the definition of  $\bar{\alpha}_i$ , we may express each  $\bar{\mathbf{c}}_i$  as

$$\begin{aligned} \bar{\mathbf{c}}_i &= \begin{bmatrix} \alpha_i \\ 1 - \alpha_i \end{bmatrix} = \bar{\alpha}_i \begin{bmatrix} \alpha_a \\ 1 - \alpha_a \end{bmatrix} + (1 - \bar{\alpha}_i) \begin{bmatrix} \alpha_b \\ 1 - \alpha_b \end{bmatrix} \\ &= \bar{\alpha}_i \bar{\mathbf{c}}_a + (1 - \bar{\alpha}_i) \bar{\mathbf{c}}_b, \end{aligned} \quad (42)$$

i.e., as a convex combination of the vectors  $\bar{\mathbf{c}}_a$  and  $\bar{\mathbf{c}}_b$ . Substituting  $\bar{\mathbf{c}}_i$  into... the RHS of (41), yields  $\mathbf{T}^{-1}\bar{\mathbf{c}}_i = \bar{\alpha}_i \mathbf{T}^{-1}\bar{\mathbf{c}}_a +$

$(1 - \bar{\alpha}_i)T^{-1}\bar{c}_b \geq 0, \forall i$ . With  $\bar{\alpha}_i$  and  $1 - \bar{\alpha}_i$  non-negative, the inequality holds if  $T^{-1}\bar{c}_a \geq 0$  and  $T^{-1}\bar{c}_b \geq 0$ . Also, if  $T^{-1}\bar{c}_i \geq 0$  for all  $i$ , then it holds for  $i = a$  and  $i = b$ . Thus,

$$T^{-1}\bar{c}_i \geq 0, \forall i \iff T^{-1}\bar{c}_a \geq 0 \text{ and } T^{-1}\bar{c}_b \geq 0. \quad (43)$$

Again, this holds for arbitrary positive scaling of each  $\bar{c}_i$ . Note that  $\alpha_a > 0$  from  $\alpha_a \geq \alpha_i, \forall i$  and  $C$  having full row-rank. Similarly,  $1 - \alpha_b > 0$ . Consider scaling  $\bar{c}_a$  by  $\frac{1}{\alpha_a}$  and  $\bar{c}_b$  by  $\frac{1}{1 - \alpha_b}$ . Then

$$\begin{aligned} T^{-1}\bar{c}_a \geq 0 &\iff T^{-1} \begin{bmatrix} 1 \\ \frac{1 - \alpha_a}{\alpha_a} \end{bmatrix} = T^{-1} \begin{bmatrix} 1 \\ \frac{c_{2a}}{c_{1a}} \end{bmatrix} \geq 0, \\ T^{-1}\bar{c}_b \geq 0 &\iff T^{-1} \begin{bmatrix} \frac{\alpha_b}{1 - \alpha_b} \\ 1 \end{bmatrix} = T^{-1} \begin{bmatrix} \frac{c_{1b}}{c_{2b}} \\ 1 \end{bmatrix} \geq 0. \end{aligned} \quad (44)$$

Note that

$$\begin{aligned} \alpha_a \geq \alpha_i, \forall i &\iff \frac{c_{2a}}{c_{1a}} = \frac{1 - \alpha_a}{\alpha_a} \leq \frac{1 - \alpha_i}{\alpha_i} = \frac{c_{2i}}{c_{1i}}, \forall i, \\ \alpha_b \leq \alpha_i, \forall i &\iff \frac{c_{1b}}{c_{2b}} = \frac{\alpha_b}{1 - \alpha_b} \leq \frac{\alpha_i}{1 - \alpha_i} = \frac{c_{1i}}{c_{2i}}, \forall i. \end{aligned} \quad (45)$$

Define  $r' = \min_i \frac{c_{2i}}{c_{1i}}$  and  $r'' = \min_i \frac{c_{1i}}{c_{2i}}$ . From (45) it holds that  $r' = \frac{c_{2a}}{c_{1a}}$  and  $r'' = \frac{c_{1b}}{c_{2b}}$ . Thus,

$$T^{-1}C^{(k)} \geq 0, \forall k \iff T^{-1} \begin{bmatrix} 1 \\ r' \end{bmatrix} \geq 0 \text{ and } T^{-1} \begin{bmatrix} r'' \\ 1 \end{bmatrix} \geq 0. \quad (46)$$

□

## REFERENCES

- [1] J. Hollis, R. Raich, J. Kim, B. Fishbain, and S. Kendler, "Foreground signature extraction for an intimate mixing model in hyperspectral image classification," in *Proc. IEEE Int. Conf. Acoust., Speech Signal Process. (ICASSP)*, 2020, pp. 4732–4736.
- [2] M. E. Winter, "N-FINDR: An algorithm for fast autonomous spectral end-member determination in hyperspectral data," in *Proc. Imag. Spectrometry V*, vol. 3753. Int. Soc. Opt. Photonics, 1999, pp. 266–275.
- [3] N. Dobigeon, S. Moussaoui, M. Coulon, J.-Y. Tourneret, and A. O. Hero, "Joint Bayesian endmember extraction and linear unmixing for hyperspectral imagery," *IEEE Trans. Signal Process.*, vol. 57, no. 11, pp. 4355–4368, Nov. 2009.
- [4] P. Ghamisi, J. Plaza, Y. Chen, J. Li, and A. J. Plaza, "Advanced spectral classifiers for hyperspectral images: A review," *IEEE Geosci. Remote Sens. Mag.*, vol. 5, no. 1, pp. 8–32, Mar. 2017.
- [5] G. Camps-Valls and L. Bruzzone, "Kernel-based methods for hyperspectral image classification," *IEEE Trans. Geosci. Remote Sens.*, vol. 43, no. 6, pp. 1351–1362, Jun. 2005.
- [6] J. M. Bioucas-Dias, "A variable splitting augmented Lagrangian approach to linear spectral unmixing," in *Proc. 1st Workshop Hyperspectral Image Signal Process.: Evolution Remote Sens.*, 2009, pp. 1–4.
- [7] R. Heylen, M. Parente, and P. Gader, "A review of nonlinear hyperspectral unmixing methods," *IEEE J. Sel. Topics Appl. Earth Observ. Remote Sens.*, vol. 7, no. 6, pp. 1844–1868, Jun. 2014.
- [8] N. Dobigeon, J.-Y. Tourneret, C. Richard, J. C. M. Bermudez, S. McLaughlin, and A. O. Hero, "Nonlinear unmixing of hyperspectral images: Models and algorithms," *IEEE Signal Process. Mag.*, vol. 31, no. 1, pp. 82–94, Jan. 2014.
- [9] S. Kendler, I. Ron, S. Cohen, R. Raich, Z. Mano, and B. Fishbain, "Detection and identification of sub-millimeter films of organic compounds on environmental surfaces using short-wave infrared hyperspectral imaging: Algorithm development using a synthetic set of targets," *IEEE Sensors J.*, vol. 19, no. 7, pp. 2657–2664, Apr. 2019.
- [10] S. Kendler et al., "Non-contact and non-destructive detection and identification of bacillus anthracis inside paper envelopes," *Forensic Sci. Int.*, vol. 301, pp. e55–e58, Aug. 2019.
- [11] S. Kendler, Z. Mano, R. Aharoni, R. Raich, and B. Fishbain, "Hyperspectral imaging for chemicals identification: A human-inspired machine learning approach," *Sci. Rep.*, vol. 12, no. 1, 2022, Art. no. 17580.
- [12] N. Keshava and J. Mustard, "Spectral unmixing," *IEEE Signal Process. Mag.*, vol. 19, no. 1, pp. 44–57, Jan. 2002.
- [13] J. Nascimento and J. Dias, "Vertex component analysis: A fast algorithm to unmix hyperspectral data," *IEEE Trans. Geosci. Remote Sens.*, vol. 43, no. 4, pp. 898–910, Apr. 2005.
- [14] D. Heinz and Chein-I-Chang, "Fully constrained least squares linear spectral mixture analysis method for material quantification in hyperspectral imagery," *IEEE Trans. Geosci. Remote Sens.*, vol. 39, no. 3, pp. 529–545, Mar. 2001.
- [15] J. W. Boardman, "Automating spectral unmixing of AVIRIS data using convex geometry concepts," in *Proc. JPL, Summaries 4th Annu. JPL Airborne Geosci. Workshop. Volume 1: AVIRIS Workshop*, 1993, pp. 4177–4193.
- [16] T.-H. Chan, W.-K. Ma, A. Ambikapathi, and C.-Y. Chi, "A simplex volume maximization framework for hyperspectral endmember extraction," *IEEE Trans. Geosci. Remote Sens.*, vol. 49, no. 11, pp. 4177–4193, Nov. 2011.
- [17] T.-H. Chan, C.-Y. Chi, Y.-M. Huang, and W.-K. Ma, "A convex analysis-based minimum-volume enclosing simplex algorithm for hyperspectral unmixing," *IEEE Trans. Signal Process.*, vol. 57, no. 11, pp. 4418–4432, Nov. 2009.
- [18] V. Leplat, A. M. Ang, and N. Gillis, "Minimum-volume rank-deficient nonnegative matrix factorizations," in *Proc. IEEE Int. Conf. Acoust., Speech Signal Process. (ICASSP)*, 2019, pp. 3402–3406.
- [19] J. Li and J. M. Bioucas-Dias, "Minimum volume simplex analysis: A fast algorithm to unmix hyperspectral data," in *Proc. IEEE Int. Geosci. Remote Sens. Symp. (IGARSS)*, vol. 3, 2008, pp. III-250–III-253.
- [20] Y. Qian, S. Jia, J. Zhou, and A. Robles-Kelly, "L1/2 sparsity constrained nonnegative matrix factorization for hyperspectral unmixing," in *Proc. Int. Conf. Digit. Image Comput.: Techn. Appl.*, 2010, pp. 447–453.
- [21] R. Rajabi and H. Ghassemian, "Spectral unmixing of hyperspectral imagery using multilayer NMF," *IEEE Geosci. Remote Sens. Lett.*, vol. 12, no. 1, pp. 38–42, 2015.
- [22] J. M. Bioucas-Dias and M. A. T. Figueiredo, "Alternating direction algorithms for constrained sparse regression: Application to hyperspectral unmixing," in *Proc. 2nd Workshop Hyperspectral Image Signal Process.: Evolution Remote Sens.*, 2010, pp. 1–4.
- [23] S. Khoshokhan, R. Rajabi, and H. Zayyani, "Sparsity-constrained distributed unmixing of hyperspectral data," *IEEE J. Sel. Topics Appl. Earth Observ. Remote Sens.*, vol. 12, no. 4, pp. 1279–1288, Apr. 2019.
- [24] S. Khoshokhan, R. Rajabi, and H. Zayyani, "Clustered multitask nonnegative matrix factorization for spectral unmixing of hyperspectral data," *J. Appl. Remote Sens.*, vol. 13, no. 2, pp. 026509–026509, 2019.
- [25] Y. Qian, F. Xiong, S. Zeng, J. Zhou, and Y. Y. Tang, "Matrix-vector nonnegative tensor factorization for blind unmixing of hyperspectral imagery," *IEEE Trans. Geosci. Remote Sens.*, vol. 55, no. 3, pp. 1776–1792, Mar. 2017.
- [26] F. Xiong, Y. Qian, J. Zhou, and Y. Y. Tang, "Hyperspectral unmixing via total variation regularized nonnegative tensor factorization," *IEEE Trans. Geosci. Remote Sens.*, vol. 57, no. 4, pp. 2341–2357, Apr. 2019.
- [27] J. M. Bioucas-Dias et al., "Hyperspectral unmixing overview: Geometrical, statistical, and sparse regression-based approaches," *IEEE J. Sel. Topics Appl. Earth Observ. Remote Sens.*, vol. 5, no. 2, pp. 354–379, Apr. 2012.
- [28] J. M. Nascimento and J. M. Bioucas-Dias, "Nonlinear mixture model for hyperspectral unmixing," in *Proc. Image Signal Process. Remote Sens. XV*, vol. 7477, 2009, pp. 157–164.
- [29] N. Yokoya, J. Chanussot, and A. Iwasaki, "Nonlinear unmixing of hyperspectral data using semi-nonnegative matrix factorization," *IEEE Trans. Geosci. Remote Sens.*, vol. 52, no. 2, pp. 1430–1437, Feb. 2014.
- [30] C. H. Ding, T. Li, and M. I. Jordan, "Convex and semi-nonnegative matrix factorizations," *IEEE Trans. Pattern Anal. Mach. Intell.*, vol. 32, no. 1, pp. 45–55, Jan. 2010.
- [31] A. Halimi, Y. Altmann, N. Dobigeon, and J.-Y. Tourneret, "Nonlinear unmixing of hyperspectral images using a generalized bilinear model," *IEEE Trans. Geosci. Remote Sens.*, vol. 49, no. 11, pp. 4153–4162, Nov. 2011.
- [32] Y. Deville, "From separability/identifiability properties of bilinear and linear-quadratic mixture matrix factorization to factorization algorithms," *Digit. Signal Process.*, vol. 87, pp. 21–33, Apr. 2019.
- [33] C. Kervaz, N. Gillis, and N. Dobigeon, "Provably robust blind source separation of linear-quadratic near-separable mixtures," *SIAM J. Imag. Sci.*, vol. 14, no. 4, pp. 1848–1889, 2021.
- [34] B. Hapke, "Bidirectional reflectance spectroscopy: 1. Theory," *J. Geophys. Res. Solid Earth*, vol. 86, no. B4, pp. 3039–3054, 1981.

- [35] A. Dixit and S. Agarwal, "Non-linear spectral unmixing of hyperspectral data using modified PPNMM," *Appl. Comput. Geosci.*, vol. 9, 2021, Art. no. 100053.
- [36] X. Lu, H. Wu, Y. Yuan, P. Yan, and X. Li, "Manifold regularized sparse NMF for hyperspectral unmixing," *IEEE Trans. Geosci. Remote Sens.*, vol. 51, no. 5, pp. 2815–2826, May 2013.
- [37] D. Donoho and V. Stodden, "When does non-negative matrix factorization give a correct decomposition into parts?" in *Proc. Adv. Neural Inf. Process. Syst.*, vol. 16, 2004, pp. 1141–1148.
- [38] H. Laurberg, M. G. Christensen, M. D. Plumbley, L. K. Hansen, and S. H. Jensen, "Theorems on positive data: On the uniqueness of NMF," *Comput. Intell. Neurosci.*, vol. 2008, May 2008.
- [39] K. Huang, N. D. Sidiropoulos, and A. Swami, "Non-negative matrix factorization revisited: Uniqueness and algorithm for symmetric decomposition," *IEEE Trans. Signal Process.*, vol. 62, no. 1, pp. 211–224, Jan. 2014.
- [40] X. Fu, K. Huang, and N. D. Sidiropoulos, "On identifiability of nonnegative matrix factorization," *IEEE Signal Process. Lett.*, vol. 25, no. 3, pp. 328–332, Mar. 2018.
- [41] S. Jia and Y. Qian, "Constrained nonnegative matrix factorization for hyperspectral unmixing," *IEEE Trans. Geosci. Remote Sens.*, vol. 47, no. 1, pp. 161–173, Jan. 2009.
- [42] L. Zhuang, C.-H. Lin, M. A. T. Figueiredo, and J. M. Bioucas-Dias, "Regularization parameter selection in minimum volume hyperspectral unmixing," *IEEE Trans. Geosci. Remote Sens.*, vol. 57, no. 12, pp. 9858–9877, Dec. 2019.
- [43] X. Fu, K. Huang, B. Yang, W.-K. Ma, and N. D. Sidiropoulos, "Robust volume minimization-based matrix factorization for remote sensing and document clustering," *IEEE Trans. Signal Process.*, vol. 64, no. 23, pp. 6254–6268, Dec. 2016.
- [44] L. Miao and H. Qi, "Endmember extraction from highly mixed data using minimum volume constrained nonnegative matrix factorization," *IEEE Trans. Geosci. Remote Sens.*, vol. 45, no. 3, pp. 765–777, Mar. 2007.
- [45] X. Fu, K. Huang, N. D. Sidiropoulos, and W.-K. Ma, "Nonnegative matrix factorization for signal and data analytics: Identifiability, algorithms, and applications," *IEEE Signal Process. Mag.*, vol. 36, no. 2, pp. 59–80, Mar. 2019.



**Jarrod Hollis** received the B.S. and M.S. degrees in electrical and computer engineering from Oregon State University, Corvallis, Oregon, in 2019 and 2023, respectively. Since 2019, he has been working toward the Ph.D. degree in computer science with the School of Electrical Engineering and Computer Science, Oregon State University, Corvallis, OR, USA. His research interests include hyperspectral imaging, and more recently theory and applications of adversarial machine learning.



**Raviv Raich** (Senior Member, IEEE) received the B.Sc. and M.Sc. degrees from Tel-Aviv University, Tel-Aviv, Israel, in 1994 and 1998, respectively, and the Ph.D. degree from the Georgia Institute of Technology, Atlanta, GA, USA, in 2004, all in electrical engineering. Between 1999 and 2000, he was a Researcher with the Communications Team, Industrial Research, Ltd., Wellington, New Zealand. From 2004 to 2007, he was a Postdoctoral Fellow with the University of Michigan, Ann Arbor. He has been with the School of Electrical Engineering and Computer Science, Oregon State University, Corvallis, as an Assistant Professor (2007–2013), Associate Professor (2013–2023), and is currently a Professor (2023–present). His research interests include probabilistic modeling and optimization in signal processing and machine learning. His co-authored papers at the IEEE MLSP workshop 2015, ICASSP 2018, and IEEE MLSP 2019 workshop received Best Paper Awards. He was an Associate Editor for the IEEE TRANSACTIONS ON SIGNAL PROCESSING from 2011 to 2014. He served as a Member (2011–2016) and then a Chair (2017–2018) of the Machine Learning for Signal Processing (MLSP) Technical Committee (TC) of the IEEE Signal Processing Society. Since 2019, he is a Member of the Signal Processing Theory and Methods (SPTM), a TC of the IEEE Signal

Processing Society. He served as a Co-Chair of the 2024 IEEE Workshop on Sensor Array and Multichannel Signal Processing.



statistical signal processing, machine learning, optimization, and smart grid.

**Jinsub Kim** (Member, IEEE) received the Ph.D. degree in electrical and computer engineering with minors in applied mathematics and statistics from Cornell University, Ithaca, NY, USA. He is currently an Associate Professor with the School of Electrical Engineering and Computer Science, Oregon State University (OSU), Corvallis. Prior to joining OSU, he was a Postdoctoral Associate with Cornell University. From 2019 to 2023, he served as a Chair of the Signal Processing Society chapter of IEEE Oregon section. His research interests include



California at Berkeley. His research interests include enviromatics, devising AI and machine learning methods and mathematical models for better understanding built and natural complex environments. The goal is to harness new machine learning and mathematical models with engineering principles, computing, and networked sensing data analytics for enhancing the efficiency, resiliency, and sustainability of infrastructure and natural systems. This includes topics related to hydro-informatics, atmospheric-informatics, traffic data, structural health, smart infrastructure systems and connected transportation.

**Barak Fishbain** is an Associate Professor with the Environmental, Water and Agricultural Engineering Division, Faculty of Civil & Environmental Engineering in the Technion-Israel Institute of Technology Haifa, Israel. Prior to his arrival to the Technion, he served as an Associate Director with the Integrated Media Systems Center (IMSC), Viterbi School of Engineering, University of Southern California (USC) and did his Postdoctoral studies with the Department of Industrial Engineering and Operations Research (IEOR), University of



He is now a Visiting Scholar with the Environmental, Water & Agricultural Engineering Division, Faculty of Civil & Environmental Engineering, Technion Israel Institute of Technology. His research interests include developing new methods for HSI data interpretation and applying them to precise agriculture.

**Shai Kendler** received the Ph.D. degree in physical chemistry from Hebrew University of Jerusalem. He studied optical and mass spectrometry of van der Waals clusters in supersonic jets. After completing his doctoral studies in 1996, he moved to Israel Institute for Biological Research, Ness Ziona Israel (IIBR). He focused on field portable detection using thermal analysis, optical, and ion mobility spectrometry. In 2005, he was a Visiting Scholar with the University of Michigan, Ann Arbor, studying MEMS for SVOC vapor separation and detection.